Comparison of Seismic Slope–Performance Models — Case Study of the Oakland East Quadrangle, California

By

Scott B. Miles[1] and David K. Keefer[2]

Open–File Report 99–137

1999

U.S. DEPARTMENT OF THE INTERIOR

U.S. GEOLOGICAL SURVEY

1 Spatial Analysis in Geotechnical Engineering Lab, Dept. Civil and Env. Engrg., Univ. of Mass., Amherst 01003, smiles@sage.ecs.umass.edu

2 Western Regions Earthquake Hazards Team, 345 Middlefield Rd., MS 977, Menlo Park, CA 94025, dkeefer@usgs.gov

Comparison of Seismic Slope–Performance Models — Case Study of the Oakland East Quadrangle, California

By

Scott B. Miles and David K. Keefer

Abstract: Researchers, emergency response and lifeline managers, and municipal planners are beginning to recognize the utility of seismic landslide hazard zonation. With this recognition, the decisions made based on resulting maps could have widespread social and economic impact in the event of a large earthquake. This report compares several popular permanent displacement models for assessing seismic slope–performance. The approaches are implemented in a raster GIS to expose potential differences and assess the effects of using a particular approach within a decision–making context. It is observed that each approach forecasts notably different levels of slope–performance. Thus, considering the variety of spatial seismic landslide analysis approaches and the effect of basing a decision on a map created using a single one of them, it is suggested that less reliance be put on the traditional paper map format. Instead, multiple approaches can be used to investigate many scenario earthquakes under a variety of conditions in a computer–based spatial decision support system.

INTRODUCTION

Keefer (1984) observed that earthquakes of moderate to high magnitude can cause landslides over an area as large as 500,000 km^2. These landslides also have large damage potential as illustrated by the recent effects of the 1989 Loma Prieta and 1994 Northridge earthquakes (Harp and Jibson, 1995; Keefer, 1998). Accordingly, researchers, emergency response and lifeline managers, and municipal planners are beginning to recognize the utility of seismic landslide hazard and risk zonation. With this recognition, the decisions made based on resulting hazard or risk maps could have widespread social and economic impact in the event of a large earthquake. Therefore, investigating and comparing several popular techniques for seismic slope–performance zonation is important.

The state of the art in seismic landslide hazard zonation using geographic information systems (GIS) was summarized by Ho and Miles (1997), who suggested several potential approaches using dynamic permanent–displacement models. In the short time since then, considerable effort has been spent improving seismic landslide hazard zonation techniques using spatial technologies (Miles and Ho, 1999; Jibson and others, 1998; McCrink and Real, 1996). This report extends the study of Ho and Miles (1997) by implementing several seismic slope–performance models using raster GIS to expose any differences between the approaches and assess the potential effects of using a particular approach within a decision–making context. The report begins by summarizing the approaches that exist for determining seismic landslide hazard. The general procedure of a permanent–displacement analysis — the class of approaches chosen in the report for investigation — is then described. The report concludes by discussing the implementation of

each individual approach and the differences among these approaches.

PERMANENT–DISPLACEMENT ANALYSIS

Three basic approaches exist for conducting seismic landslide hazard analysis. These consist of the statistical, pseudo–static, and permanent–displacement approaches. A statistical approach assesses hazard by assuming the past predicts the future. Hazard is assessed through correlation of past landslides with several influential factors. Results of a statistically based analysis can range from an estimated probability of failure to some index indicating degrees of hazard. Pseudo–static analysis employs a traditional static slope–stability analysis with the addition of a horizontal force component that models the effects of earthquake–induced ground–motions. A pseudo–static analysis yields a factor of safety against seismic slope failure. This effectively provides a simple binary index of whether a slope is expected to fail or not at a given level of seismic acceleration. Permanent–displacement techniques provide information regarding actual slope–performance through calculation of some index of relative or actual displacement based on commonly accepted characterizations of earthquake–shaking severity. Permanent–displacement analysis is chosen for investigation because of its higher information content, better modeling of ground–motion, and increasing acceptance in the earthquake engineering community.

Newmark's Sliding Block Analogy

In his landmark paper, Newmark (1965) noted that the transient effects of earthquake motions can cause permanent deformation of slopes prior to complete failure. Newmark proposed modeling a slope subjected to earthquake–induced accelerations as a friction block resting on an inclined plane subjected to the same accelerations as the modeled slope (Figure 1). Therefore, in each instance when the sum of the static and dynamic forces exceed the shear resistance of the sliding interface the block will displace. The interface shear resistance is commonly characterized by the critical acceleration (a_c) of the modeled slope, which is the base acceleration needed to overcome the shear resistance. Newmark (1965) defined the following relationship to calculate critical acceleration in the case of planar slip:

$$a_c = (FS - 1)\sin\alpha \qquad (1)$$

where FS is the static factor of safety of the slope and α is the thrust angle of the landslide block, which can be approximated by the slope angle. Total induced displacement can be determined by summing the displacement resulting from each instance the shear resistance is exceeded during ground shaking. This value must be evaluated to assess the potential effect on the landslide block. Newmark displacements should be considered indices that indicate relative slope–performance during seismic shaking rather than a precise prediction of slope deformation (Jibson and others, 1998). Thus, to define the related hazard (i.e. Damage potential) a probability of failure should be determined through correlation with actual landslides or by using a relationship, such as the one presented in Jibson and others (1998).

The sliding block analogy assumes the slope is rigid and perfectly plastic and that shear strength remains constant during shaking. Each assumption may only be valid for certain conditions and does not represent general behavior. For example, assuming rigid, perfectly

plastic behavior will result in an over–estimation of Newmark displacement for strain–hardening materials and an under–estimation for strain–softening materials (Kramer, 1996). However, a Newmark analysis has the advantage over more recent developments in permanent–displacement analysis (i.e. Finite element and finite difference techniques) in that the only additional information beyond that required for static slope–stability analysis is an appropriate acceleration time history. Whereas with the more advanced approaches, require defining several constitutive parameters and can require a prohibitive amount of material testing for regional slope–performance analysis.

Double Integration Approach

Newmark originally employed an energy–based method for calculating cumulative slope displacement. A less numerically cumbersome method was developed by Wilson and Keefer (1983) where those parts of an earthquake accelerogram that exceed the critical acceleration of a slope are double–integrated (Figure 2). The numerical scheme is straightforward to implement as illustrated by routines existing in BASIC, FORTRAN and C (Jibson, 1993; Sharma, 1996; Miles, 1997). Even so, application of the double–integration algorithm can require significant time and computing resources when used for spatial–analysis.

The two major steps of the double–integration approach are calculation of the critical acceleration of each slope of interest and selection of an appropriate earthquake time history. Selection of a time history for predictive hazard analysis can pose a major obstacle in using the double–integration approach. Ideally, records of an earthquake that occurred on the fault zone of interest having adequate magnitude are used. Unfortunately in many — if not most — cases, such records do not exist. The alternatives consist of modifying actual records from the fault zone of interest (or another fault system) or generating artificial time histories. This issue is treated in greater detail by Miles and Ho (1999) and Kramer (1996).

Simplified Approach

Citing the numerical complexity and the difficulty associated with selection of acceleration time histories, a handful of researchers have developed simplified approaches to calculating Newmark displacements (Franklin and Chang, 1977; Makdisi and Seed, 1978; Ambraseys and Menu, 1988; Yegian and others, 1991; Jibson, 1993; Jibson and others, 1998). By and large, these approaches are based on numerical regression of results obtained from double–integrating real or synthetic time histories. Variations among approaches are typically in the ground–motion descriptors used to correlate with Newmark displacement and in the final means with which to conduct the simplified analysis. Simplified approaches that are chart based are clumsy and imprecise when applied to regional analysis and, thus, are not considered in this report. The balance of the simplified approaches take the form of simple mathematical equations, which are developed from regression analyses. It is relatively straightforward to apply any of the approaches that follow this style to slope–performance zonation.

SUBJECT LOCATION

In order to compare the various slope–performance analyses when applied to a real–life

problem, the 7.5 minute 1:24,000 Oakland East quadrangle, California was selected as the region on which to conduct seismic slope–performance zonation. This particular area has been the subject of previous seismic landslide studies (Herbel, 1994; Miles and Barrera, unpub. Data, 1995; Miles and Ho, 1999). The Oakland East quadrangle is located in the San Francisco Bay area and contains the eastern parts of the cities of Oakland and Berkeley (Figure 3). The quadrangle is bisected by the Hayward fault, the predominant seismic source in the region, which strikes southeast–northwest. The hilly areas northeast of the fault exhibit moderate to steep slopes (Figure 4). Because of the large amount of existing infrastructure and areas of dense population, seismic landslide hazard within the Oakland East quadrangle is of great interest to lifeline managers and municipal planners.

SEISMIC SLOPE–PERFORMANCE ZONATION Four approaches to seismic slope–performance zonation using Newmark's analysis were implemented using raster GIS. The majority of the models were applied using the Arc/Info GRID module, which facilitates algebraic manipulation of raster coverages (i.e. Map or grid algebra). All analysis was performed at a 10–meter resolution. All of the approaches follow the same general procedure. The four steps involved are data collection, seismic landslide susceptibility assessment, seismic shaking characterization, and lastly, permanent–displacement analysis. The various approaches differ in the methods used in conducting the latter two steps. The implementation of the four different approaches are discussed later in this section. The common steps of data collection and seismic landslide susceptibility assessment are described below in reverse order.

Seismic Landslide Susceptibility Analysis and Data Collection

Regional susceptibility to earthquake–triggered landslides can be assessed by determining the critical acceleration of each slope in the area. In the case of spatial–analysis using GIS, this is typically done for each pixel in the coverage. As previously noted, determination of critical acceleration requires the calculation of the static factor of safety for each slope. The most common approach to conducting regional static slope–stability analysis is to apply the infinite slope model to each pixel in the coverage. However, neighborhood analysis can be employed to account for inter–pixel interaction. Such a method is referred to as a focal analysis, as opposed to local analysis where each pixel is treated individually. Using the infinite slope model, the static factor of safety of a slope (FS) can be expressed as:

$$FS = \frac{c'}{\gamma d \sin\alpha} + \frac{\tan\phi'}{\tan\alpha} + \frac{m\gamma_w \tan\phi'}{\gamma \tan\alpha} \qquad (2)$$

where c' is the effective cohesion, ϕ' is the effective angle of internal friction, γ is the material unit weight, γ_w is the unit weight of water, α is the angle of the slope from the horizontal, d is the normal depth to the failure surface, and m is a ratio of d indicating the location of the ground water table. For this report, a local analysis using the infinite slope model was conducted. The slope–stability analysis was performed for completely dry (m=0) and saturated (m=1) conditions to bound possible water table elevations in lieu of real data.

The data collection step comprises gathering representative values for each parameter of the infinite slope model. This step is crucial to the remaining steps of any permanent–displacement analysis. Even so, as the goal of this report is the comparison of slope–performance models,

simple estimates of material property values were used. Therefore, the resulting slope–performance maps presented later in this report are not fit for use as a critical decision–making tool. Material property estimates were made during a previous study of the Oakland East quadrangle (Miles and Barrera, unpub. Data, 1995). Soil strength values were produced through overlay of the engineering geology map (Radbruch 1969) and the USDA soil survey map of the quadrangle (Welch, 1981). USCS classifications specified in the soil survey were assigned to each geologic unit polygon. Thus, different polygons of the same geologic unit could have different USCS classifications. Actual values were then obtained using relationships of friction angle or cohesion to USCS classification from Bell (1981), the NAVFAC Design Manual, and engineering judgment. This approach will underestimate strength in areas where soils are shallow and sliding occurs in the underlying bedrock. However, static stability was ensured for all slopes in the analysis area. The areal distribution of estimates for drained cohesion and friction angle are shown in Figures 5 and 6, respectively.

The final two parameters needed to perform a seismic landslide susceptibility analysis are slope angles and the depth to failure for each potential landslide (pixel). Slope angles were calculated from a USGS format 1:24,000 10–meter DEM of the Oakland East quadrangle. For estimation of landslide failure depth, a single value of 10 feet was assumed throughout the quadrangle. The value of 10 feet is considered representative for the most abundant types of earthquake–induced landslides (Keefer, 1984). Based on the data collected, maps showing the areal distribution of critical acceleration under dry and saturated conditions were produced for use in subsequent Newmark analysis. The maps are shown in Figures 7 and 8, respectively.

Ambraseys and Menu (1988)

One of the first well–known simplified approaches to Newmark's analysis was developed by Ambraseys and Menu (1988). They developed a suite of regression equations based on actual ground–motion records that express Newmark displacement (D_N) as a function of critical acceleration ratio, which is the ratio of critical acceleration (a_c) to peak ground acceleration (a_{max}). The equation used for this report does not consider up–slope movement and is expressed as:

$$\log D_N = 0.90 + \log\left[\left(1 - \frac{a_c}{a_{max}}\right)^{2.53}\left(\frac{a_c}{a_{max}}\right)^{-1.09}\right] \quad (3)$$

When critical acceleration ratio is greater than one, the result will be complex. Application of the model requires that peak ground accelerations (PGA) be calculated for the coverage. This was accomplished using the attenuation relationship of Abrahamson and Silva (1997) as suggested in Sitar and Khazai (unpub. Data). For moment magnitudes (M) greater than 6.4 the relationship takes the following form:

$$\ln a_{max} = 0.828 - 0.144(M - 6.4) - 0.102(8.5 - M)^2 + [0.838 + 0.17(M - 6.4)]\ln R \quad (4)$$

where a_{max} is expressed in units of gravity and R is epicentral distance in kilometers. In order to apply the attenuation relationship, the distance to the epicenter must be calculated for each pixel in the coverage. This was accomplished by digitizing the trace of the Hayward fault from Radbruch (1969) and calculating the euclidean distance between each pixel and the nearest point on the fault trace using the GRID function *EUCDISTANCE*. This approach does not explicity yield the epicentral distance, rather the distance to fault–rupture, because the epicenter is not known for the scenario earthquake. PGA was calculated for a scenario **M**=7 earthquake. Because of the near–field limitations of the attenuation relationship, the minimum epicentral distance was set to 1 kilometer. Attenuation of PGA is shown in Figure 9. With PGA calculated, it was then a simple matter to calculate Newmark displacements from the critical acceleration maps created for dry and saturated conditions. The seismic slope–performance maps created are shown for dry and saturated conditions in Figures 10 and 11.

Yegian and others (1991)

To address the inability of PGA as the sole descriptor of seismic shaking to explicitly consider frequency content and duration, Yegian and others (1991) developed an expression for calculating median normalized Newmark displacement (D_N^*). Newmark displacements were calculated for the regression analysis by double–integrating 348 time histories of actual earthquakes, which were compiled by Franklin and Chang (1977).

$$\log \dot{D_N} = \log\left[\frac{D_N g}{a_{max} N_{eq} T^2}\right] = 0.22 - 10.12\left(\frac{a_c}{a_{max}}\right) + 16.38\left(\frac{a_c}{a_{max}}\right)^2 - 11.48\left(\frac{a_c}{a_{max}}\right)^3 \qquad \textbf{(5)}$$

In the equation, N_{eq} is an equivalent number of cycles and T is the predominant period of the input motion. To employ this model, values for these two parameters needed to be selected. The mean number of equivalent cycles for an **M**=7 earthquake is approximately 8 according to Seed and others (1975). Based on Seed and others (1969), the predominant period at rock outcrops for distances less then 40 kilometers is approximately 0.30 seconds. Maps depicting Newmark displacements for dry (Figure 12) and saturated (Figure 13) conditions were then produced using the PGA map described above.

Jibson and others (1998)

Recognizing that PGA tends to correlate poorly with earthquake damage, Jibson (1993) developed an equation based on Arias intensity (I_a) to better characterize the damaging effects of ground–motion. Jibson (1993) also noted the general lack of agreement among simplified approaches which are based on critical acceleration ratio. The regression equation was calibrated by double–integrating eleven acceleration time histories, including ten from California, with Arias intensities less than 10 $^{m}/_{s}$ over a range of critical acceleration values (0.02 – 0.40g). The equation was later updated using 555 records from 13 earthquakes (Jibson and others, 1998). The form of the equation was also altered to make the critical acceleration term logarithmic, thus reducing the sensitivity to critical acceleration noted by Miles and Ho (1999). The equation takes the form:

$$\log D_N = 1.521 \log I_a - 1.993 \log a_c - 1.546 \quad (6)$$

To forecast the areal distribution of Arias intensity for a **M=7** earthquake on the Hayward fault, the attenuation relationship of Wilson and Keefer (1985) was used as suggested by Jibson (1993). The following equation yields Arias intensity in meters per second.

$$\log I_a = M - 2\log\sqrt{R^2 + h^2} - 4.1 \quad (7)$$

The parameter R is as defined previously and h is the focal depth in kilometers. A representative value for San Francisco Bay area earthquakes of 10 kilometers was chosen for calculating the map of Arias intensity shown in Figure 14. Newmark displacements were calculated based on the areal distribution of Arias intensities for dry and saturated conditions. The respective maps are shown in Figures 15 and 16.

Miles and Ho (1999)

As mentioned above, the simplified approaches to Newmark's analysis were created from the motivation to reduce the numerical complexity associated with the double–integration algorithm. This motivation seems doubly important in the case of spatial hazard analysis. However, the ever increasing power of computer processors, the advent of parallel processing, and the speed of low–level programming languages in fact makes the simplification of numerics less of a priority. In addition, the tendency to use a single ground–motion predictor rather than acceleration time histories reduces much of the advantage of a permanent–displacement analysis over the pseudo–static approach. Considering this, Miles and Ho (1999) applied the double–integration algorithm of Wilson and Keefer (1983) for calculating Newmark displacements to a 30 km^2 area of the East Bay Hills, which lie within the Oakland East quadrangle.

In the study of Miles and Ho (1999), input time histories were generated using the stochastic simulation developed by Boore (1983). Artificial accelerograms were used in lieu of actual records from the Hayward fault of adequate size and because of the short–comings associated with scaling earthquake records from other seismic zones. The first step of the simulation involves windowing Gaussian white noise having zero mean. The transient noise is then transformed to the frequency domain and multiplied by a theoretical amplitude spectrum (Hanks and McGuire 1981). The simulated Fourier spectrum is then transformed back to the time domain. Because of the stochastic nature of the simulation, several realizations of the simulation must be run in order to obtain a stable prediction.

For this report, a C program called NMGRID was written for conducting spatial seismic landslide hazard analysis using the double–integration approach. The program requires ASCII formatted grid files that can be output by most commercial GIS. The program cycles through the pixels of the supplied critical acceleration grid, double–integrating the appropriate time history at each step. The time history is programmatically selected from a set of time histories — supplied as ASCII text files — based on the source to site distance value of the current pixel — supplied as part of an ASCII grid. An ASCII grid of Newmark displacements is output for importing into any GIS for map production or further hazard or risk analysis.

To avoid the time–consuming task of performing the double–integration analysis a number of

times as suggested by Boore (1983), the set of random numbers that yielded mean displacements for the test area of Miles and Ho (1999) was used for this report. Thus, a single suite of acceleration time histories for an **M**=7 earthquake occurring at a 10 kilometer pseudo–depth were generated for every 500 meter interval away from the Hayward fault. The simulation parameters used are listed in Table 1 and reflect parameters suggested for Northern California earthquakes (Boore, 1996). Application of the double–integration method to the 10–meter resolution quadrangle took about eight hours to complete each analysis on a Sun Microsystems Ultra 1 170MHz. In contrast, the simplified methods required only a few minutes. The seismic slope–performance forecasted using the double–integration approach is shown in the maps of Figures 17 and 18 for dry and saturated conditions, respectively.

DISCUSSION

With seismic slope–performance maps created using the three simplified approaches and the double–integration approach of Miles and Ho (1999), it is possible to compare potential discrepancies among the approaches. The objective of this report is to reveal any differences between the four approaches and assess the potential effects of using a particular approach over another. Thus, the maps created using each approach are visually compared. Such qualitative comparison will assist in determining the effects of using such maps as a visual tool in a decision–making process. The approaches are then compared using a statistical analysis to better quantify the discrepancies among them.

Beginning by comparing the two simplified approaches that are calibrated using PGA, it is apparent that the two models predict similar distributions but notably different levels of Newmark displacement for both dry and saturated conditions. Even more notable is that the maps created using Yegian and others (1991) have a visibly greater amount of orange to red pixels, that is, pixels having greater than ten centimeters of Newmark displacement. The difference is most obvious for the maps depicting saturated conditions. The difference in slope–performance is also effectively illustrated by the total mean displacement for each model and respective condition (Table 2). The mean resulting from the method of Ambraseys and Menu (1988) is 2.22 and 13.17 centimeters, respectively, for dry and saturated conditions. The corresponding values for Yegian and others (1991) are 6.89 and 44.74 centimeters. Both approaches were performed using the same PGA maps. The only difference in parameterization is that of the predominant period and equivalent cycles used with Yegian and others (1991). The values used were admittedly conservative. An observation regarding the Ambraseys and Menu approach that is not visibly discernible is that it does not result in any pixels having zero displacement. This is an obvious side–effect of the log–linear form of the regression equation.

Based on a different ground–motion descriptor, it would be logical to expect a difference between the Jibson and others (1998) approach and the previous two PGA–based approaches. This expectation is born out for both dry and saturated conditions. Whereas between the PGA based approaches the distribution of Newmark displacements are only subtly different, the maps produced using the Jibson and others (1998) approach show noticeably different distributions. The average Newmark displacements for the Jibson and others (1998) maps, both dry and saturated, are 1.42 and 10.72 centimeters. Thus, the approach appears to forecast lower Newmark displacements on average even though it predicts greater areal extent. Similar to the Ambraseys and Menu (1988) model, the Jibson and others (1998) model takes on a logarithmic

form. This may explain the large areas having Newmark displacement less than 2 centimeters. Also noteworthy of the Jibson and others (1998) maps is the slightly greater increase in Newmark displacements on average from dry to saturated conditions when compared to the PGA–based maps.

The final comparison is that between the double–integration approach using simulated accelerograms (Miles and Ho, 1999) and the simplified approaches. It would be expected that maps created using the simplified approaches bear a resemblance to those from the double–integration approach. This is because each simplified approach was, in some way, developed by double–integrating earthquake accelerograms. Note, however, that actual earthquake records were used in these instances. There is a general similarity between the double–integration and simplified maps. Yet, markedly different distributions and magnitudes of Newmark displacement are evident. Having average Newmark displacements of 1.03 and 9.34 centimeters for dry and saturated conditions, the Miles and Ho (1999) approach results in the lowest average predicted Newmark displacements (Table 2). Interesting however, is the magnitude increase of Newmark displacement, on average, from dry to saturated conditions. This is the greatest increase of any of the approaches and suggests a significant dependency on critical acceleration as that is the only parameter that varies with ground water conditions. The approach of Jibson and others (1998) exhibits the second largest increase. Examination of the two PGA–based approaches reveals obvious bands of hazard in the respective maps (Figures 10, 11, 12, 13) that parallel the Hayward fault. This may indicate an unrealistic influence by PGA attenuation. The fact that the Jibson and others (1998) and Miles and Ho (1999) approaches do not exhibit pronounced banding supports the conclusion that Arias intensity correlates better with Newmark displacement (Jibson, 1993).

To provide an easier and quantitative means of comparing the four approaches, cumulative distribution functions for each Newmark displacement map were calculated and plotted in Figures 19 and 20. The plots show the probability of exceedance for a given value of Newmark displacement, as predicted by each Newmark analysis. Tables 3 and 4 list the exceedance probabilities for Newmark displacements of 2, 5, and 10 centimeters to assist in the interpretation of the cumulative distribution plots. For dry conditions (Figure 19), each approach exhibits distributions of similar shape. The approach of Jibson and others (1998) predicts the greatest probability for values of Newmark displacement less than 1.5 centimeters and the least probability for displacements greater than 5 centimeters (Table 3). However, the approach does not yield the lowest maximum predicted displacement (Table 2). The approach of Miles and Ho (1999) predicts the lowest probabilities for displacements less than 5 centimeters. The two PGA–based approaches yield significantly greater probabilities for Newmark displacements greater than 5 centimeters, with the approach of Yegian and others (1991) predicting the higher probabilities. For saturated conditions (Figure 20), the relative differences between the distributions are similar to those for dry conditions. Notice however, that the distributions do not exhibit as pronounced a reduction in probability for higher values of displacement. This reflects the increase in overall Newmark displacements for saturated conditions as observed with the slope–performance maps.

The cumulative distribution plots show that the magnitude of Newmark displacements predicted by each approach differ significantly. And although the shape of the distributions are similar, there is still discernible distinction between them. This discrepancy seems to be a

function of the ground–motion model used. Three different ground–motions models were employed and there are correspondingly three distinct distributions. This observation can be most readily made using the cumulative distribution plot for dry conditions (Figure 19). Thus, the means of modeling the particular ground–motion parameter used by each approach is likely to have a significant effect on predicted regional Newmark displacements. The cumulative distribution plots also illustrate the difficulty in interpreting analysis results in map form. It appears that the maps produced using the approach of Jibson and others (1998) is more conservative than those produced using the Miles and Ho (1999) approach. And in fact, the average Newmark displacements are higher. However, the cumulative distribution plots show that the Jibson and others (1998) approach predicts lower probabilities for Newmark displacement values greater than 5 centimeters. To make an assessment of which approach predicts greater hazard, the associated probability of failure must be evaluated.

The comparison of the four approaches is based on the use of three different ground–motion models. Thus, a true comparison of the approaches can only be accomplished by using a single model of ground–motion. This of course is not possible with simple attenuation relationships. However, by calculating the Arias intensity of each simulated time history generated for use with the double–integration approach, Miles and Ho (1999) were able to make a true comparison between the Jibson (1993) model and the double–integration approach. The results showed an even larger discrepancy, with the Jibson model forecasting larger magnitudes of Newmark displacement. It is reasonable to expect that the results corresponding to the models of Ambraseys and Menu (1988) and Yegian and others (1991) follow these findings.

The disagreement among the approaches that was observed in the discussion above has the potential to greatly effect any decision–making process. For example, a pipeline manager may want to locate areas of poor seismic slope–performance in order to identify pipes to be retrofitted against earthquake–triggered landslides. Taking the two approaches that exhibited the most extreme difference — the Miles and Ho (1999) approach and the approach of Yegian and others (1991) — it is apparent that use of one approach over another can have significant economic effects. If for instance, only the Yegian and others (1991) approach was employed to map seismic slope–performance, a potentially larger number of pipes would be slated for modification.

With the increasing popularity of GIS and spatial–analysis, it is equally likely that results of a regional Newmark analysis be used as a component in other GIS–based models, for example, probability of slope failure (i.e. Hazard) or infrastructure damage (i.e. Risk). In applications such as these, the effects of using a particular seismic slope–performance model are more uncertain. The effects would depend on the hazard or risk model used and the spatial–analysis technique employed to implement the model (e.g. focal or local analysis). What is certain is that whatever the difference may be, it will be carried through each subsequent analysis. Thus, if spatial coverages of Newmark displacements are passed on to outside parties for further spatial–analysis, it is important that quality metadata (information about data and analysis) is not only maintained but transferred and exploited (Miles and Ho, 1999b).

SUMMARY & CONCLUSION

Several permanent–displacement approaches to seismic slope–performance analysis were

presented. These approaches were applied through spatial–analysis to produce Newmark displacement maps for both dry and saturated conditions. The maps resulting from each approach were compared to reveal the discrepancies and assess the potential effects of using one approach in place of another in a decision–making context. Although the comparisons indicated significant differences between the approaches, no effort was made to identify the "correct" approach. Of course, the double–integration algorithm of Wilson and Keefer (1983) forms the basis from which all the approaches compared in this report were derived. The approach of Miles and Ho (1999) directly implements the double integration algorithm. However, the validity of their particular implementation is no more certain than the other approaches because the ground motion time histories used were artificial and may not accurately depict actual ground motions in all instances. Of course, it would be a simple matter to use actual earthquake time histories if available. Further, the double–integration algorithm is quite costly with respect to processing time, and so the approach may not be practical for application to large areas. Rather, as suggested in Miles and Ho (1999), a progressive analysis technique should be employed. This consists of using simplified approaches to identify areas of moderate to poor slope–performance, which are then more thoroughly investigated using the double–integration approach using actual or artificial accelerograms.

This report only considered Newmark displacement approaches to seismic slope–performance zonation. It is also possible that a statistical or pseudo–static approach be used. Although these approaches were not considered, it is reasonable to conclude that the results will be different from the approaches presented here. This widespread disagreement is understandable since it is unlikely that any universal seismic slope–performance analysis exists for all seismic zones and input conditions. A significant reason for this is the difficulty in accurately characterizing potential seismic shaking. Another important issue, although not directly related to the specific approach, is the quality of the material property data used to conduct a hazard analysis. The cost of performing material testing on a regional scale can be prohibitive, and test data compiled from many disparate sources may not provide any significant improvement over simpler estimates (Keefer and Miles, unpub. Data, 1999).

Considering the variety of approaches to assessing seismic slope–performance and the effect of basing a decision on single one of them, it seems that the solution is to move away from reliance on the medium of static maps. Instead, multiple models can be used to investigate many scenario earthquakes under a variety of conditions in a computer–based spatial decision support system (SDSS). In this way, a decision–maker can quickly and conveniently determine the different levels of seismic slope–performance as forecasted by any number of zonation approaches. Alternatively, a single approach can be employed with a variety of ground motion models. Results of such investigations can then be extended to assess related hazard and risk. Currently, work is being done to develop a standalone SDSS that is able to implement any seismic slope–performance, landslide hazard, or landslide risk model to investigate multiple scenarios and conditions (Miles and others, 1999). With this tool, the differences that exist between approaches can be exploited to make better and more educated decisions.

REFERENCES

Abrahamson, N. A. and Silva, W. J., 1997, Equations for estimating horizontal response spectra and peak acceleration from Western North America earthquakes: A summary of recent work:

Seismological Research Letters, v. 68, no.1, p. 128–153.

Ambraseys, N.N. and Menu, J.M., 1988, Earthquake–induced ground displacements: Earthquake Engineering and Structural Dynamics, v. 16, p. 985–1006.

Bell, Frederic G., 1981, Engineering Properties of Soils and Rocks: Boston: Butterworths.

Boore, D.M., 1983, Stochastic simulation of high frequency ground motions based on seismological models of the radiated spectra: Seismological Society of America Bulletin, v. 73, no. 6, p. 1865–1894.

Franklin, A.G. and Chang, R.K., 1977, Permanent displacements of earth embankments by newmark's sliding block analysis: Report 5, Miscellaneous Paper S–71–17, U.S. Army Corps of Engineers: W.E.S. Vicksburg, MI.

Hanks, T.C. and McGuire, R.K., 1981, The character of high frequency strong ground motion, Seismological Society of America Bulletin: v. 71, no. 6, p. 2071–2095.

Harp, E.L. and Jibson, R.W. , 1995, Inventory of landslides triggered by the 1994 Northridge, California earthquake: U.S. Geological Survey Open–File Report 95–213, 17 p, 2 pl.

Herbel, W.A., 1994, Development of a GIS based landslide hazard map: Washington State University, M.S. thesis.

Ho, C.L., and Miles, S.B., 1997, Deterministic zonation of seismic slope instability: an application of GIS: ASCE Geotechnical Special Publication No. 67: Spatial Analysis in Soil Dynamics and Earthquake Engineering, p. 87–102.

Jibson, R.W., Harp, E.L., and Michael, J.A., 1998, A method for producing digital probabilistic seismic landslide hazard maps: an example from the Los Angeles, California area: U.S. Geological Survey Open–File Report 98–113, 17 p., 2 pl.

Jibson, R.W., 1993, Predicting earthquake–induced landslide displacements using Newmark's sliding block analysis: Transportation Research Record 1411, p. 9–17.

Keefer, David K. ed., 1997, The Loma Prieta, California, earthquake of October 17, 1989 — landslides: U.S. Geological Survey Professional Paper 1551–C, 183 p.

Keefer, David K., 1984, Landslides caused by earthquakes: Geological Society of America Bulletin, 95, p. 406–421.

Kramer, Steven L., 1996, Geotechnical Earthquake Engineering: New Jersey: Prentice Hall, 653 p.

Makdisi, F.I. and Seed, H.B. (1978) "Simplified procedure for estimating dam and embankment earthquake–induced deformations: Journal of the Geotechnical Engineering Division, ASCE, v. 104, no. GT3, p. 299–321.

McCrink, T.P., and Real, C.R., 1996, Evaluation of the Newmark method for mapping earthquake–induced landslide hazards in the Laurel 7.5′ quadrangle, Santa Cruz County, California: Final Technical Report for U.S. Geological Survey Contract 143–93–G–2334, 47 p.

Miles, S.B. and Ho, C.L., 1999, Rigorous landslide hazard zonation using Newmark's method and stochastic ground motion simulation: Soil Dynamics and Earthquake Engineering (in press).

— 1999b, Applications and issues of GIS in civil engineering modeling: Journal of Computing in Civil Engineering, ASCE (in press).

Miles, S.B., Keefer, D.K., and Ho, C.L., 1999, Seismic landslide hazard analysis: from hazard map to decision support system: Proceedings of the U.S. Conference on Lifeline Earthquake Engineering: Seattle, WA, August, 1999 (abstract accepted).

Miles, S.B., 1997, Rigorous landslide hazard zonation using Newmark's method and stochastic ground motion simulation: University of Massachusetts, M.S. thesis, 104 p.

Newmark, N.M., 1965, Effects of earthquakes on dams and embankments, Geotechnique, v. 15, p. 139–160.

Radbruch, D.H., 1969, Areal engineering geology of the Oakland East quadrangle, U.S. Geological Survey Map GQ–769.

Seed, H.B., Mori, K., and Chan, C.K., 1975, Influence of seismic history on the liquefaction characteristics of sands: Earthquake Engineering Research Center report 75–25, University of California at Berkeley.

Seed, H.B., Idriss, I.M., and Kiefer, F.W., 1969, Characteristics of rock motions during earthquakes, Journal of Soil Mechanics and Foundations Division, American Society of Civil Engineers, no. 95, SM5, p. 1199–1218.

Sharma, Sunil., 1996, Chap 6: Slope Stability and Stabilization Methods, Abramson, L.W., Lee, T.S., Sharma, S., and Royce, G.M (eds.). New York: Wiley, p. 408–424.

Welch, L.E., 1981, Soil survey of alameda county, California, Western Part: U.S. Department of Agriculture, Soil Conservation Service, 103 p.

Wilson, R.C. and Keefer, D.K., 1985, Predicting areal limits of earthquake–induced landsliding: U.S. Geological Survey Professional Paper 1360, p. 317–494.

Wilson, R.C. and Keefer, D.K., 1983, Dynamic analysis of a slope failure from the 6 August, 1979 Coyote Lake, California, earthquake: Seismological Society of America Bulletin, v. 73, no. 3, p. 863–877.

Yegian, M.K., Marciano, E., and Ghahraman, V.G., 1991, Earthquake–induced permanent deformations: probabilistic approach: Journal of Geotechnical Engineering, ASCE, v. 17, no. 1, p. 35–50.

Table 1. Parameters used to conduct Boore (1983) simulation.

$\Delta\sigma$, stress drop	70 bars
f_{max}, cutoff frequency	15.9 Hz
β, shear wave velocity	3.8 km/sec
ρ, density	2.8 g/cm^3
F, free surface factor	2
$R_{\theta\phi}$, radiation pattern	0.55
V, energy partition factor	0.71
B*, near–surface factor	2.3

Table 2. Summary statistics of Newmark displacement maps for dry and saturated conditions.

Approach	Mean (cm)	σ (cm)	Min. (cm)	Max. (cm)
Ambraseys and Menu (1988): Dry	2.22	8.66	0.08	308.35
Ambraseys and Menu (1988): Wet	13.17	45.15	0.10	520.97
Yegian and others (1991): Dry	6.89	34.72	0.00	1250.25
Yegian and others (1991): Wet	44.74	170.63	0.00	1607.57
Jibson and others (1998): Dry	1.42	5.59	0.09	311.35
Jibson and others (1998): Wet	10.72	44.35	0.12	598.93
Miles and Ho (1999): Dry	1.03	6.14	0.00	129.60
Miles and Ho (1999): Wet	9.34	32.64	0.00	268.00

Table 3. Dry conditions: Probability of exceeding three different Newmark displacements as predicted by the four permanent displacement approaches.

Dry	Miles and Ho (1999)	Jibson and others (1998)	Ambraseys and Menu (1988)	Yegian and others (1991)
2 cm	10%	16%	21%	29%
5 cm	4%	3%	13%	19%
10 cm	2%	1%	5%	14%

Table 4. Saturated conditions: Probability of exceeding three different Newmark displacements as predicted by the four permanent displacement approaches.

Saturated	Miles and Ho (1999)	Jibson and others (1998)	Ambraseys and Menu (1988)	Yegian and others (1991)
2 cm	28%	40%	36%	41%
5 cm	20%	18%	27%	33%
10 cm	14%	11%	21%	25%

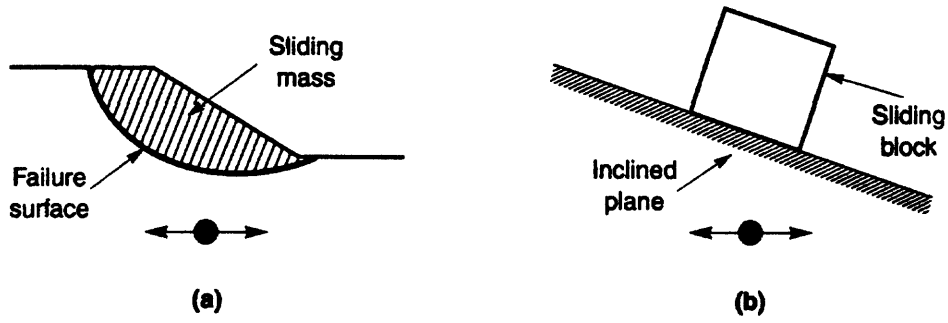

Figure 1. Newmark's (1965) sliding block analogy. The slope is modeled as friction block resting on an inclined plane subjected to the same earthquake accelerations as the modeled slope. Displacement of the block occurs when the interface shear resistance is exceeding by the sum of the static and dynamic forces (Kramer, 1996).

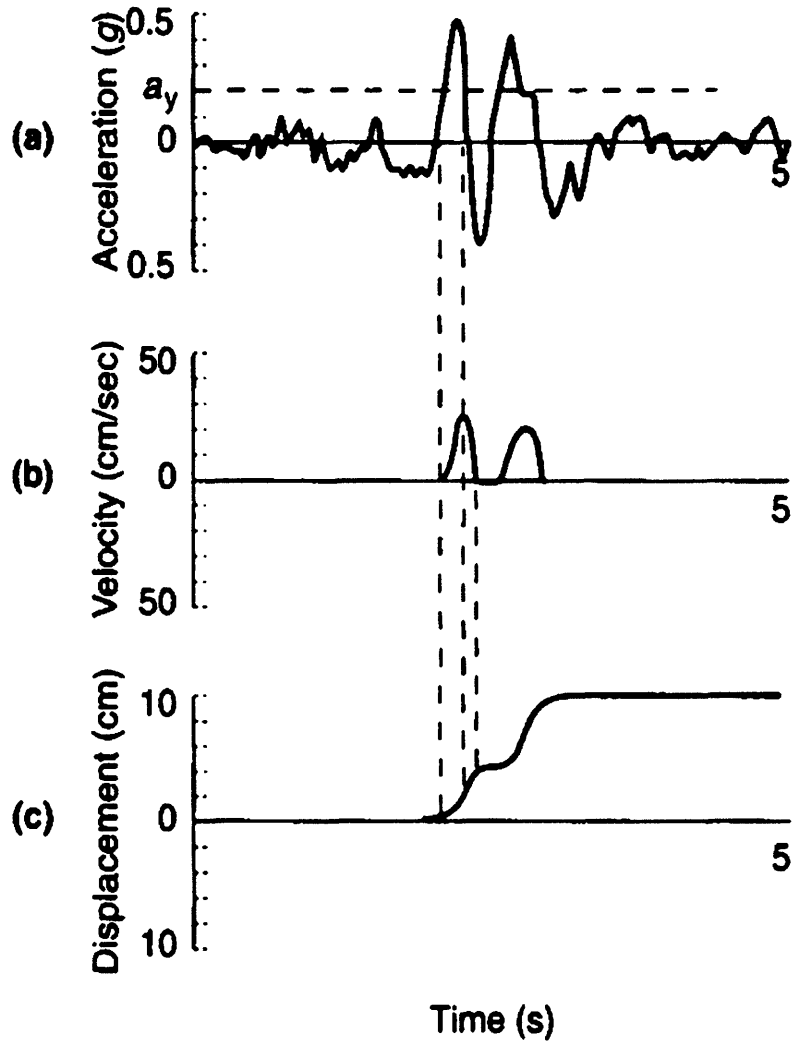

Figure 2. Example of the double-integration approach of Wilson and Keefer (1983). The critical acceleration is superimposed on an earthquake time history (a). The areas exceeding the critical acceleration are integrated to obtain the velocity time history (b) and integrated a second time to obtain cumulative displacement (c) of the sliding block.

Figure 3. Location of the Oakland East quadrangle, California. The quadrangle is in the San Francisco Bay area and contains the eastern parts of the cities of Berkeley and Oakland (Base map, Microsoft ©).

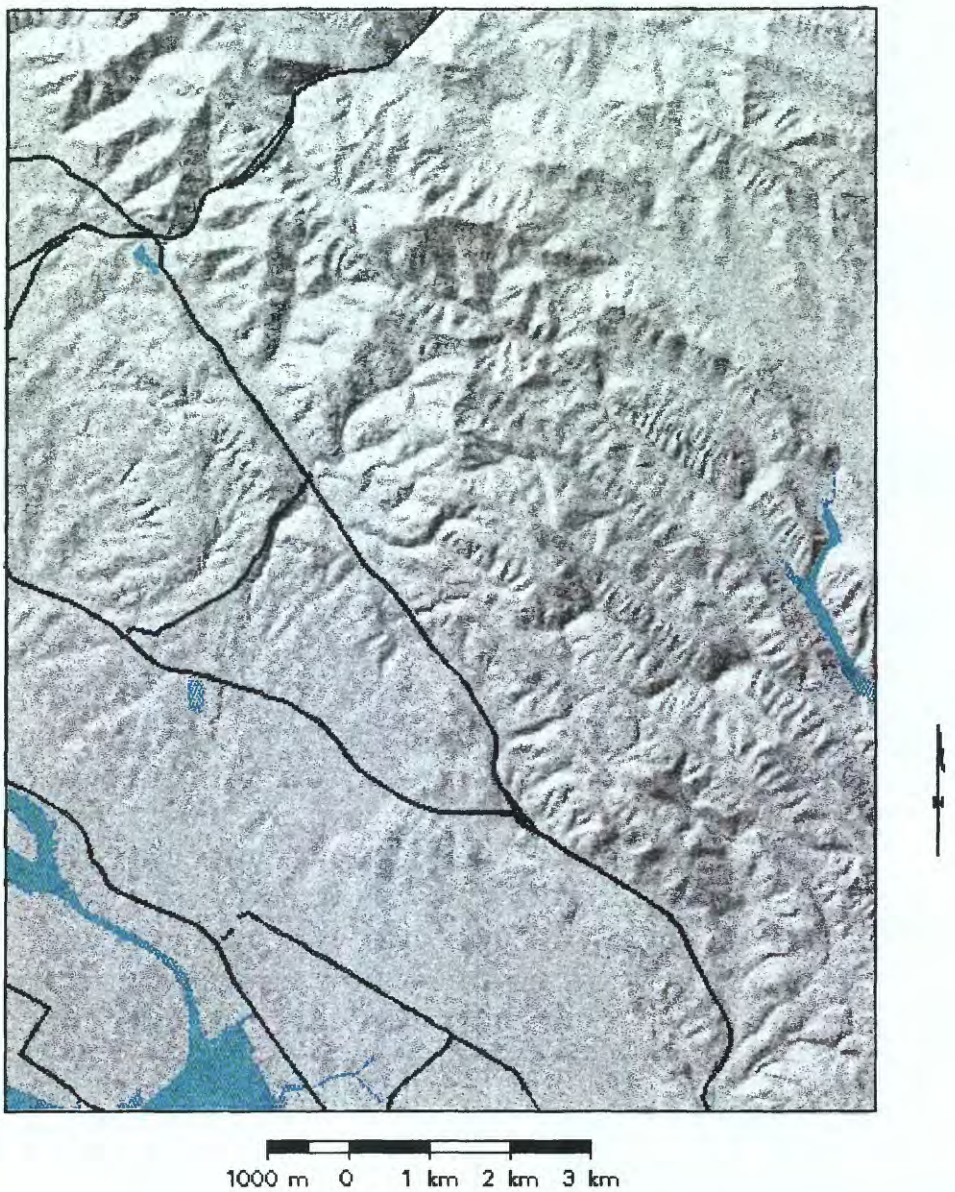

Figure 4. Shaded relief of the Oakland East quadrangle 10 meter digital elevation model (DEM). Major roads shown in black.

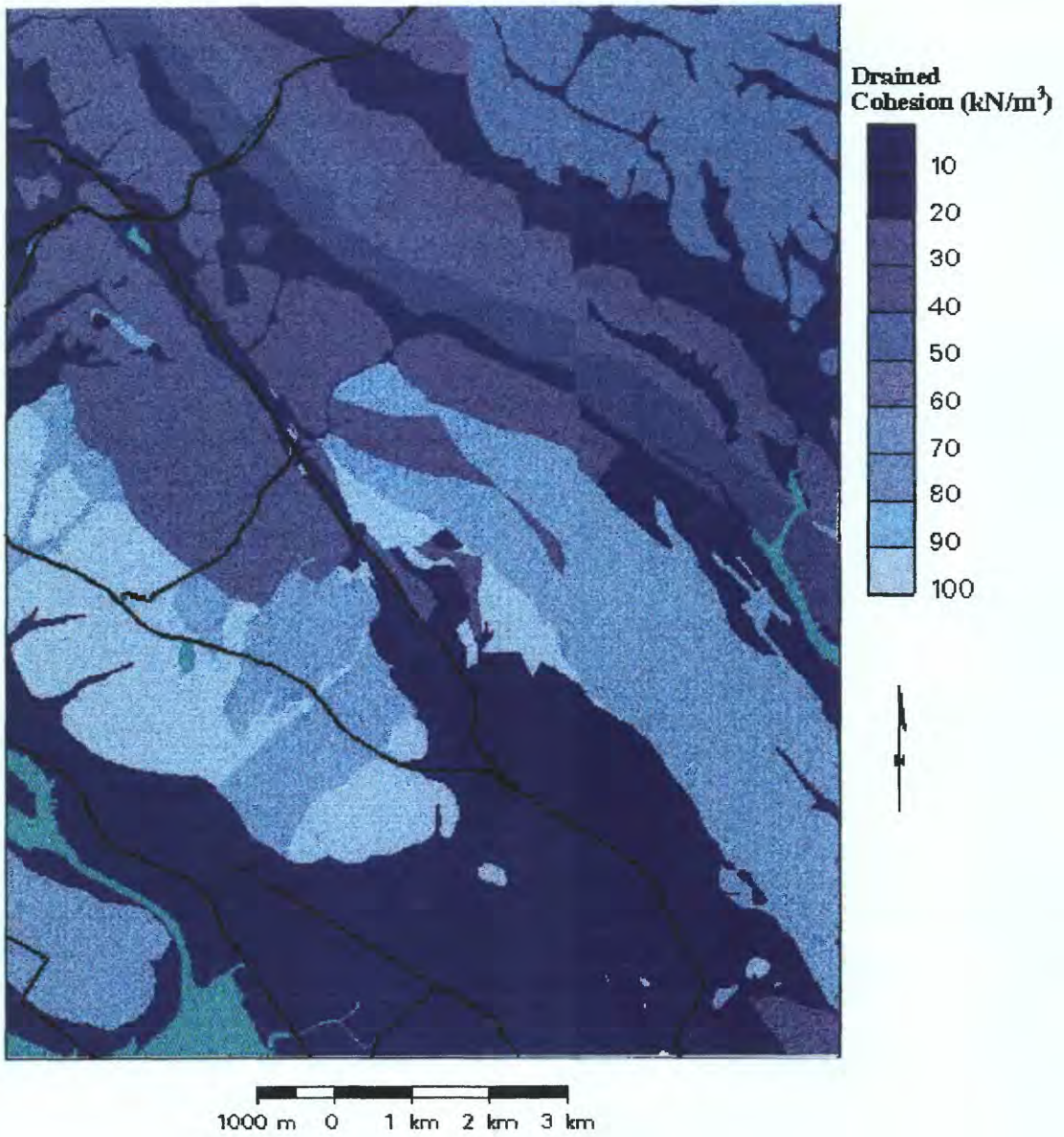

Figure 5. Map showing estimated drained cohesion assigned to the geologic units of the Oakland East quadrangle. Major roads shown in black.

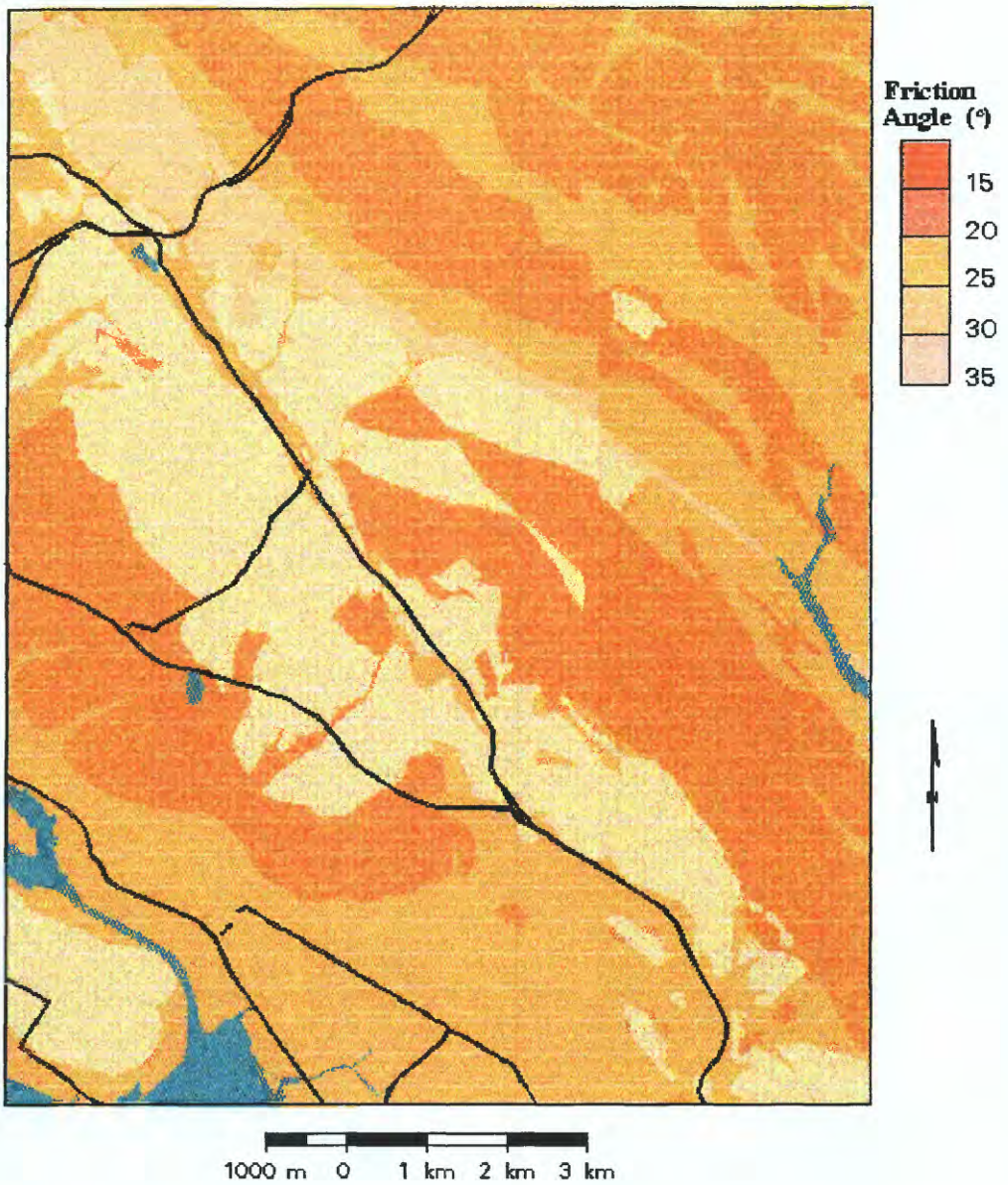

Figure 6. Map showing estimated internal angle of friction assigned to the geologic units of the Oakland East quadrangle. Major roads shown in black.

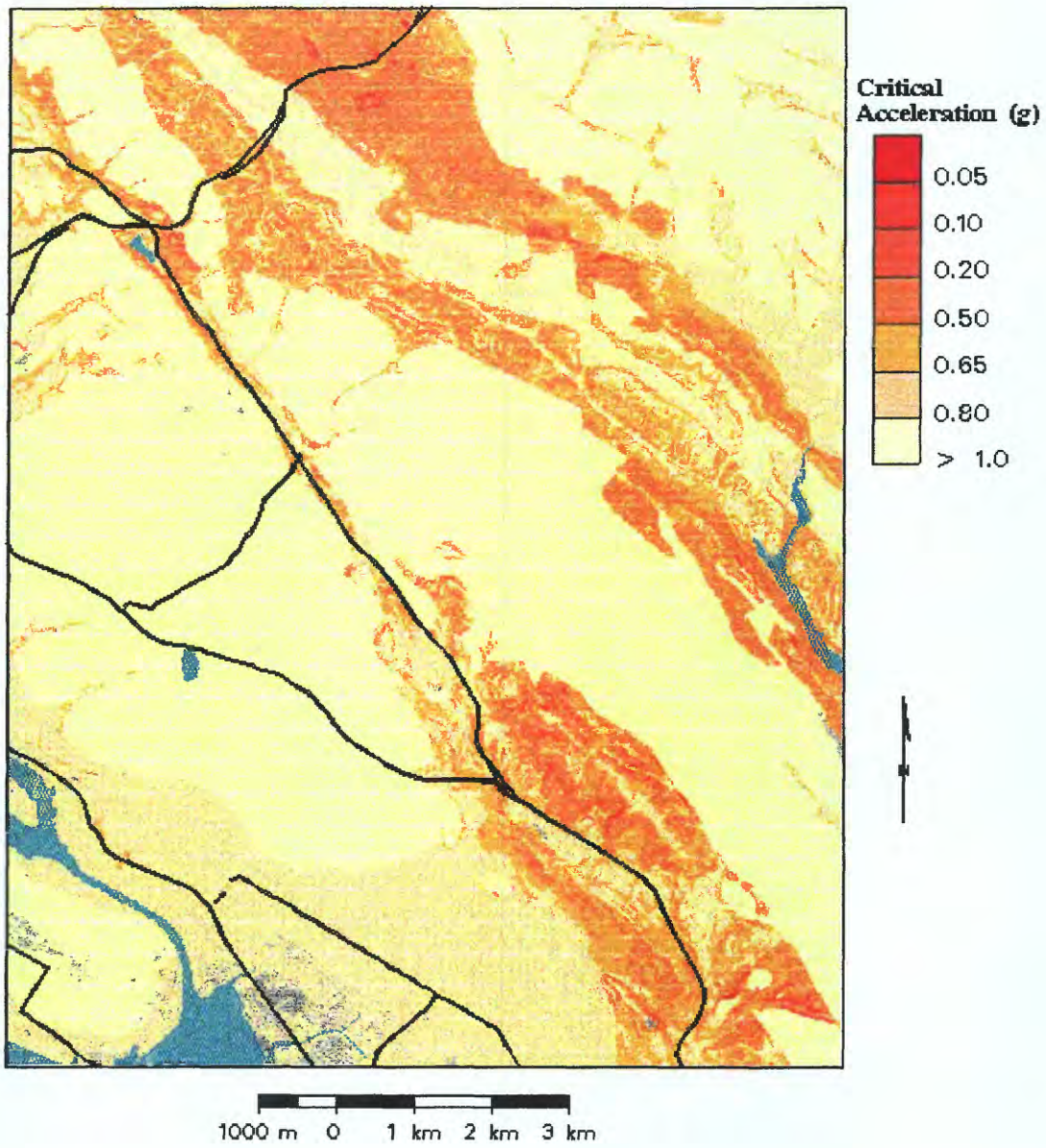

Figure 7. Map showing critical acceleration distribution under dry conditions for the Oakland East quadrangle. Major roads shown in black.

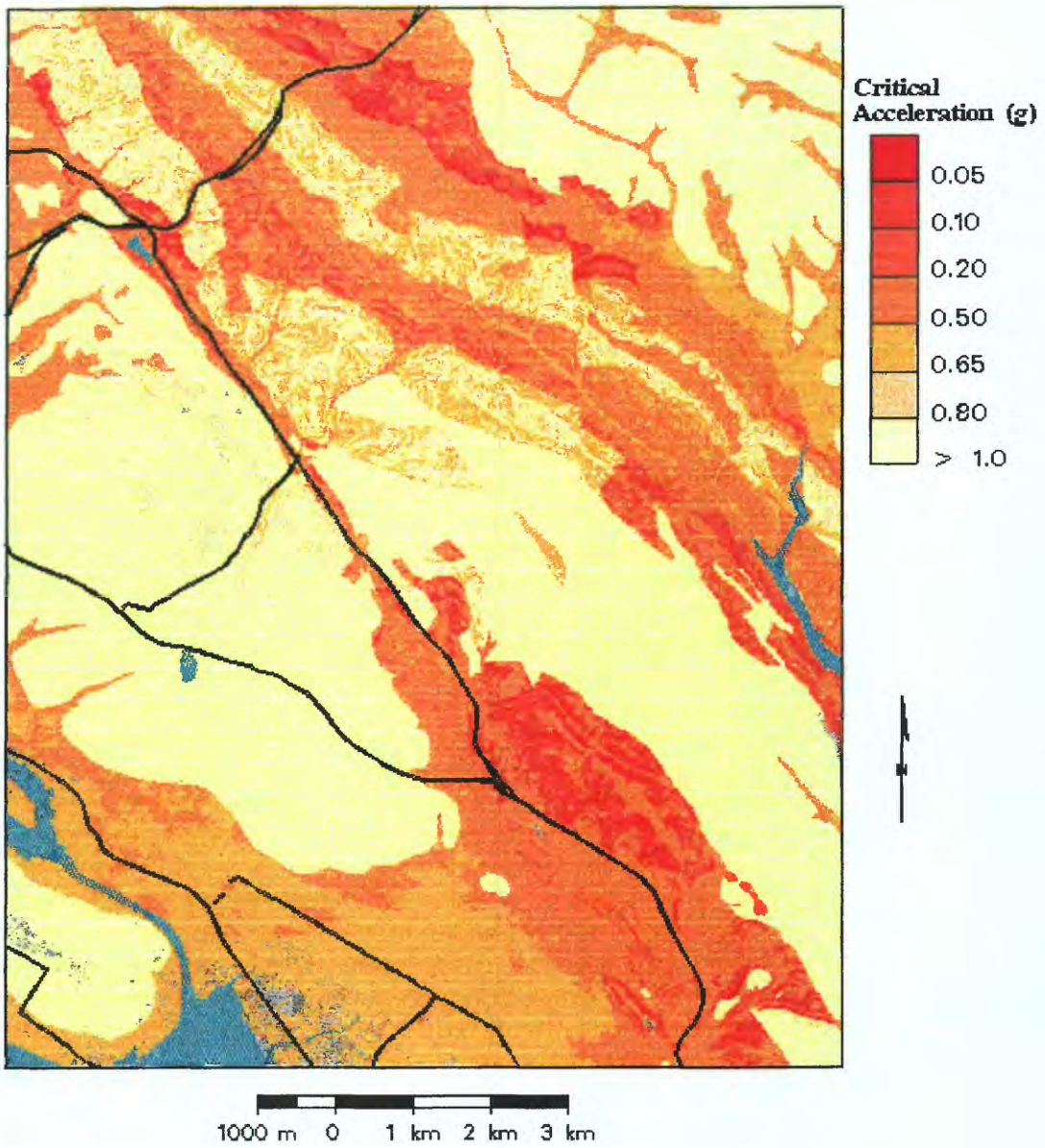

Figure 8. Map showing critical acceleration distribution under saturated conditions for the Oakland East quadrangle. Major roads shown in black.

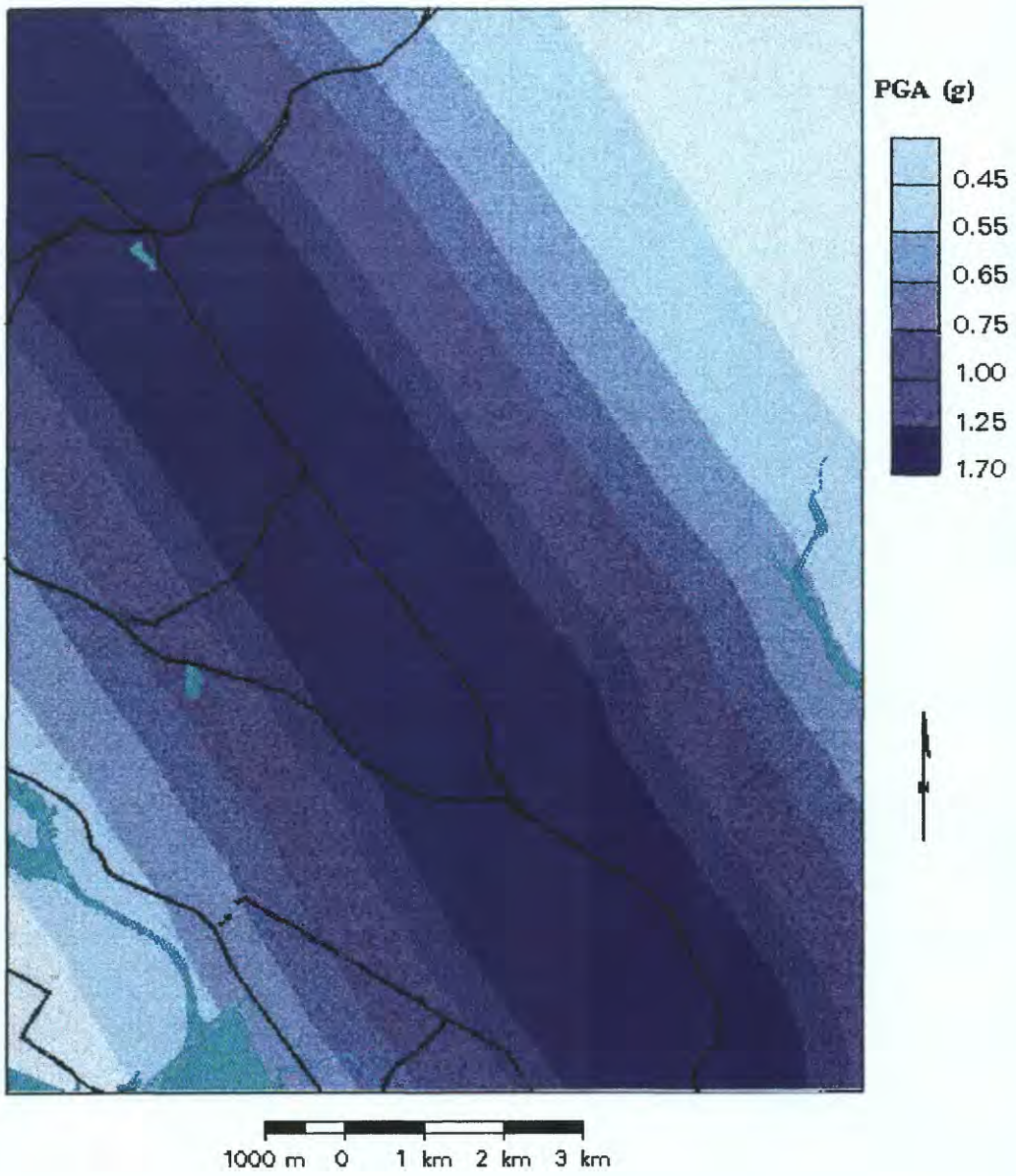

Figure 9. Map showing attenuation of peak ground acceleration (PGA) in the Oakland East quadrangle. PGA calculated for a scenario M=7 earthquake occurring on the Hayward fault, which strikes southeast–northwest. Major roads shown in black.

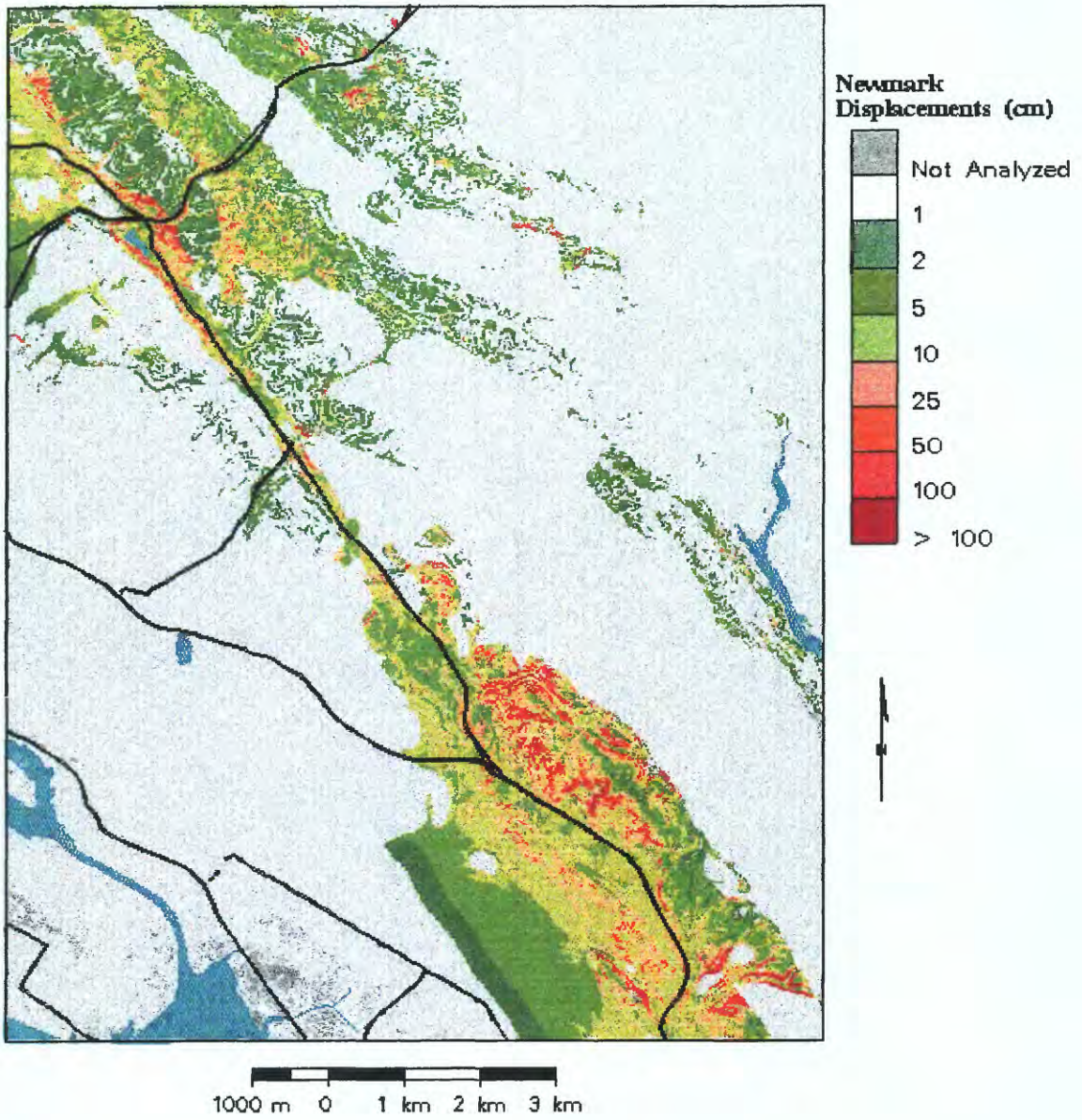

Figure 10. **Ambraseys and Menu (1988): dry conditions.** Map showing predicted Newmark displacements under dry conditions for the Oakland East quadrangle using the simplified approach of Ambraseys and Menu (1988). Newmark displacements predicted for a **M=7** scenario earthquake on the Hayward fault, California. Major roads shown in black.

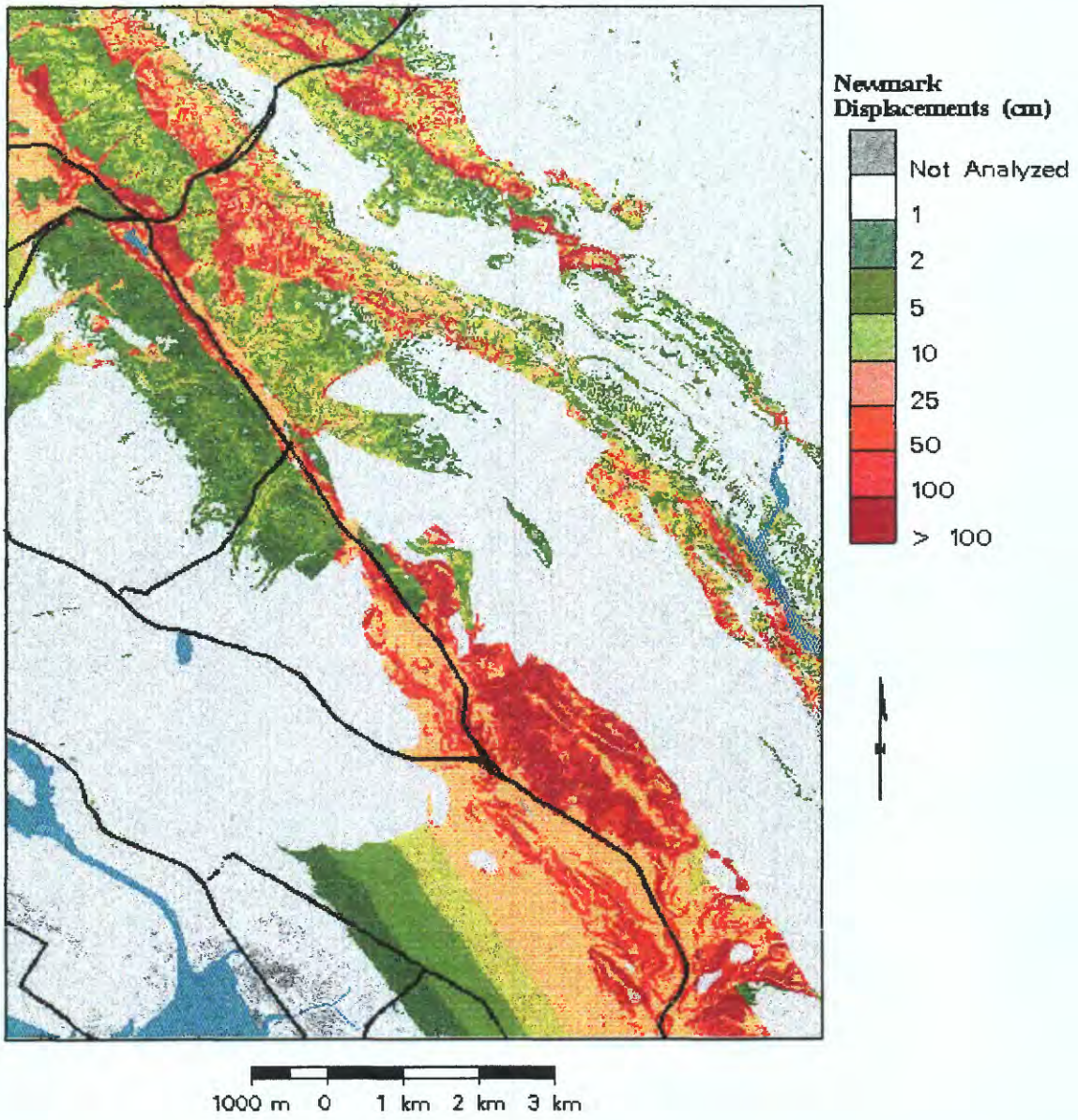

Figure 11. **Ambraseys and Menu (1988): saturated conditions.** Map showing predicted Newmark displacements under saturated conditions for the Oakland East quadrangle using the simplified approach of Ambraseys and Menu (1988). Newmark displacements predicted for a M=7 scenario earthquake on the Hayward fault, California. Major roads shown in black.

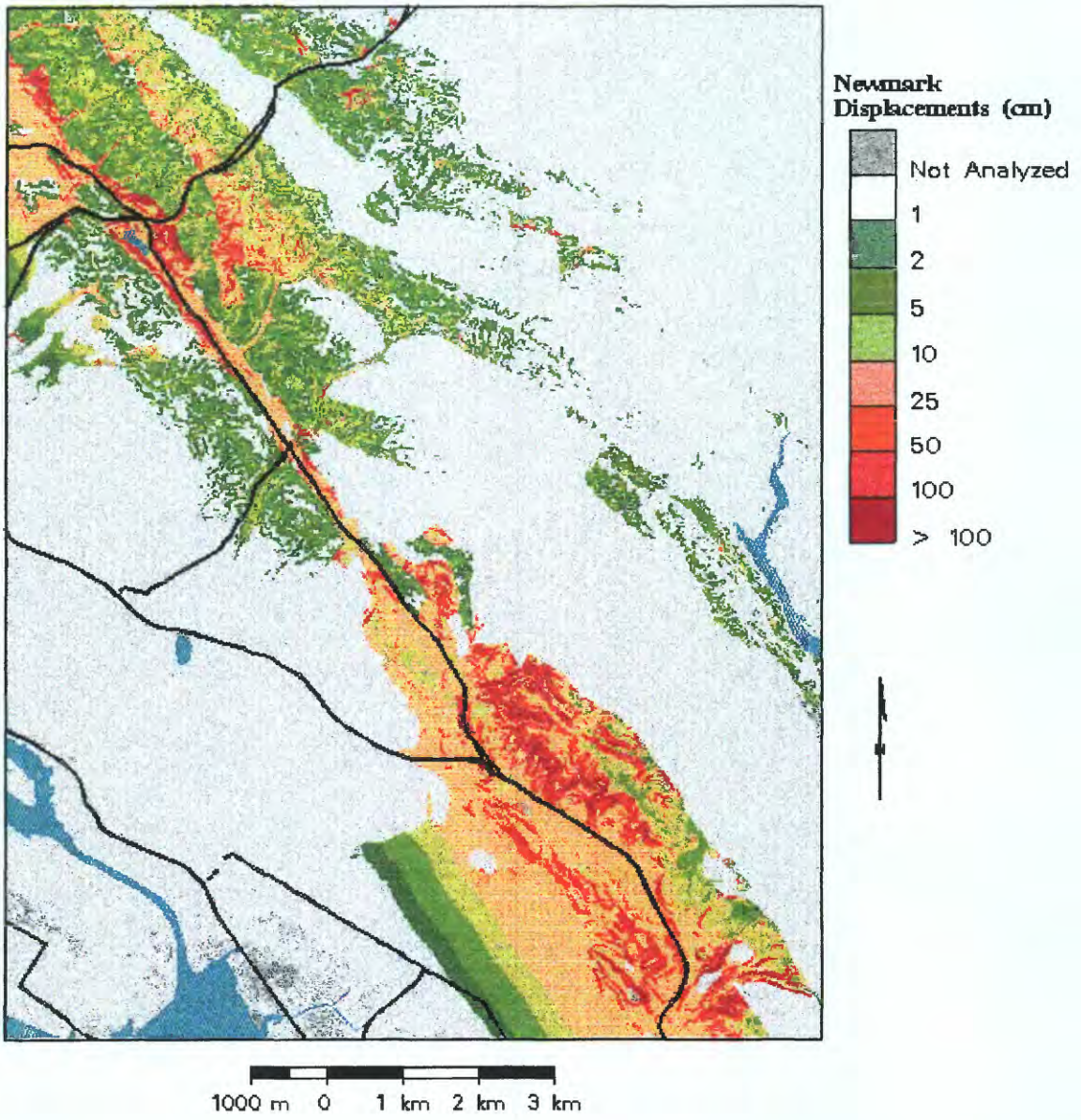

Figure 12. **Yegian and others (1991): dry condtions**. Map showing predicted Newmark displacements under dry conditions for the Oakland East quadrangle using the simplified approach of Yegian and others (1991). Newmark displacements predicted for a **M**=7 scenario earthquake on the Hayward fault, California. Major roads shown in black.

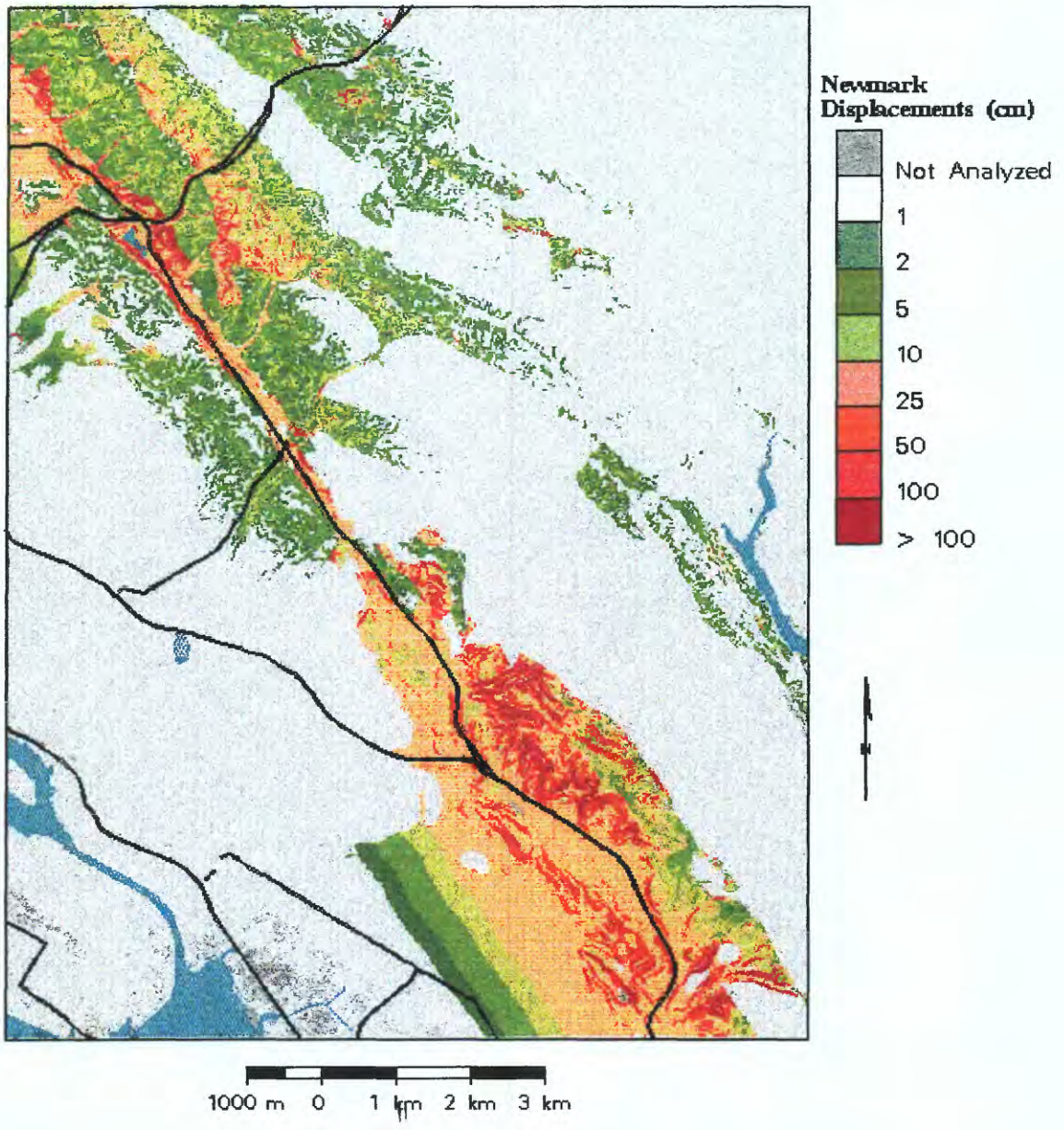

Figure 13. **Yegian and others (1991): saturated conditions.** Map showing predicted Newmark displacements under saturated conditions for the Oakland East quadrangle using the simplified approach of Yegian and others (1991). Newmark displacements predicted for a **M**=7 scenario earthquake on the Hayward fault, California. Major roads shown in black.

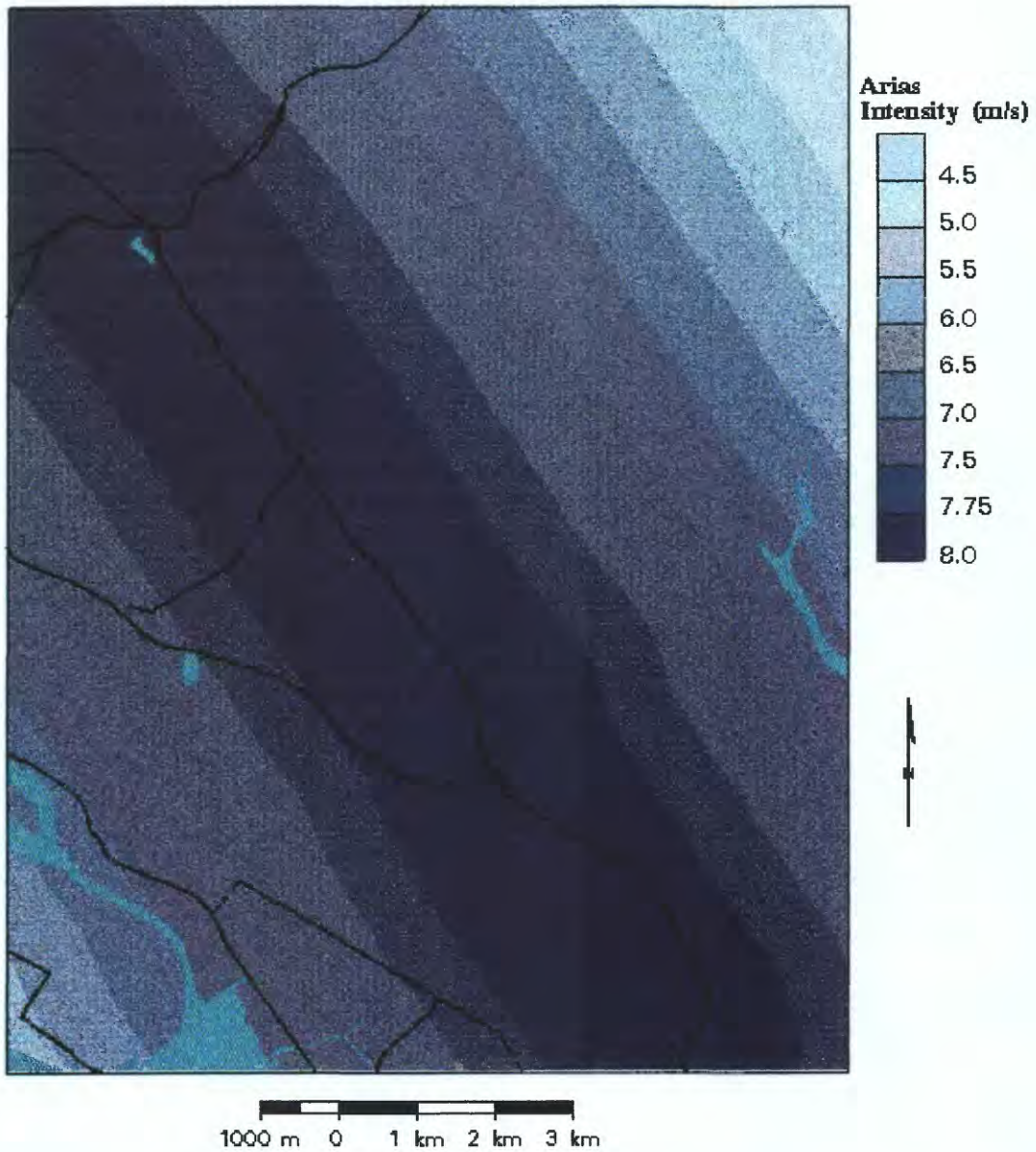

Figure 14. Map showing attenuation of Arias intensity in the Oakland East quadrangle. Arias intensity calculated for a scenario M=7 earthquake occurring on the Hayward fault, which strikes southeast–northwest. Major roads shown in black.

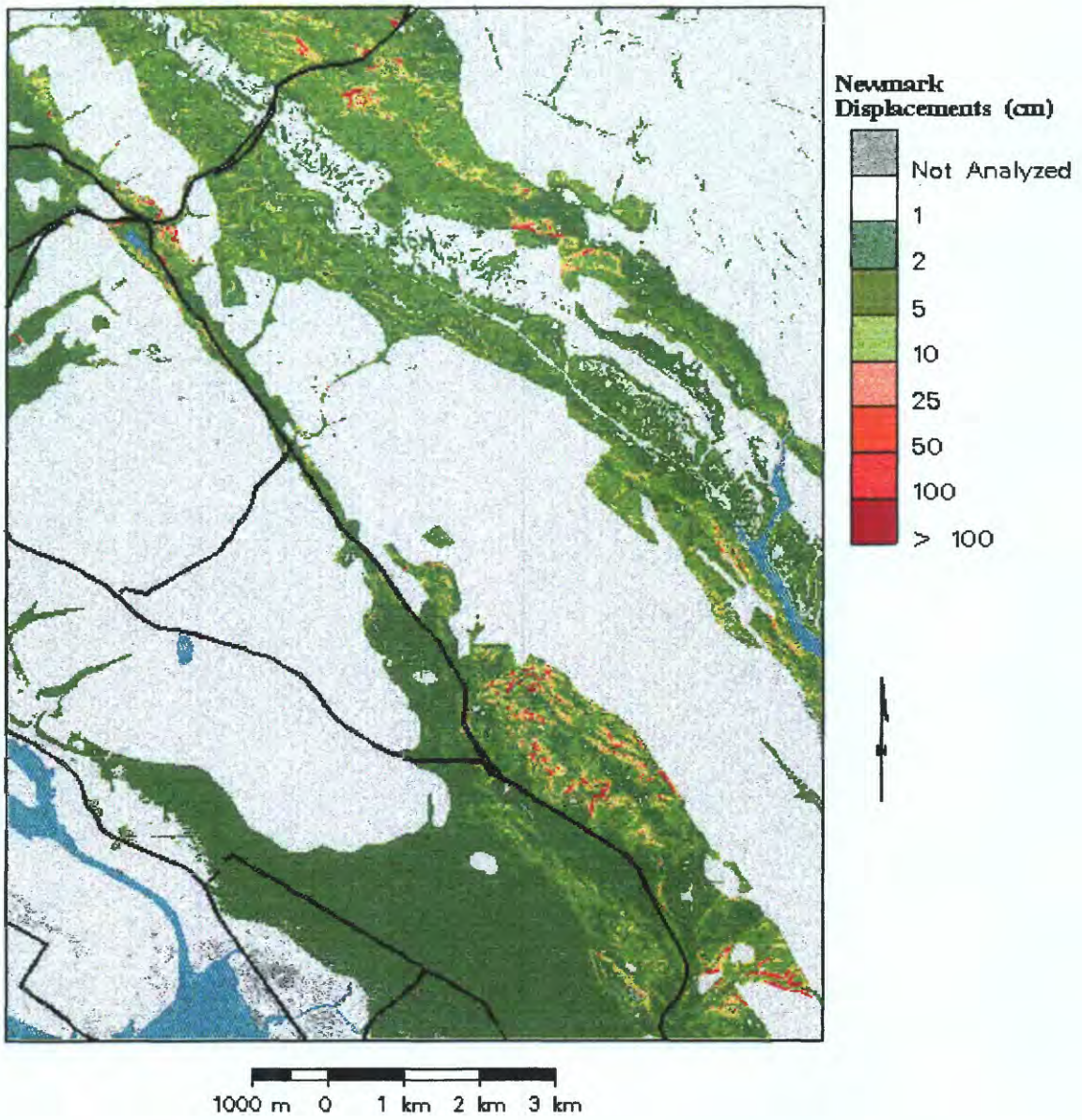

Figure 15. **Jibson and others (1998): dry conditions.** Map showing predicted Newmark displacements under dry conditions for the Oakland East quadrangle using the simplified approach of Jibson and others (1998). Newmark displacements predicted for a M=7 scenario earthquake on the Hayward fault, California. Major roads shown in black.

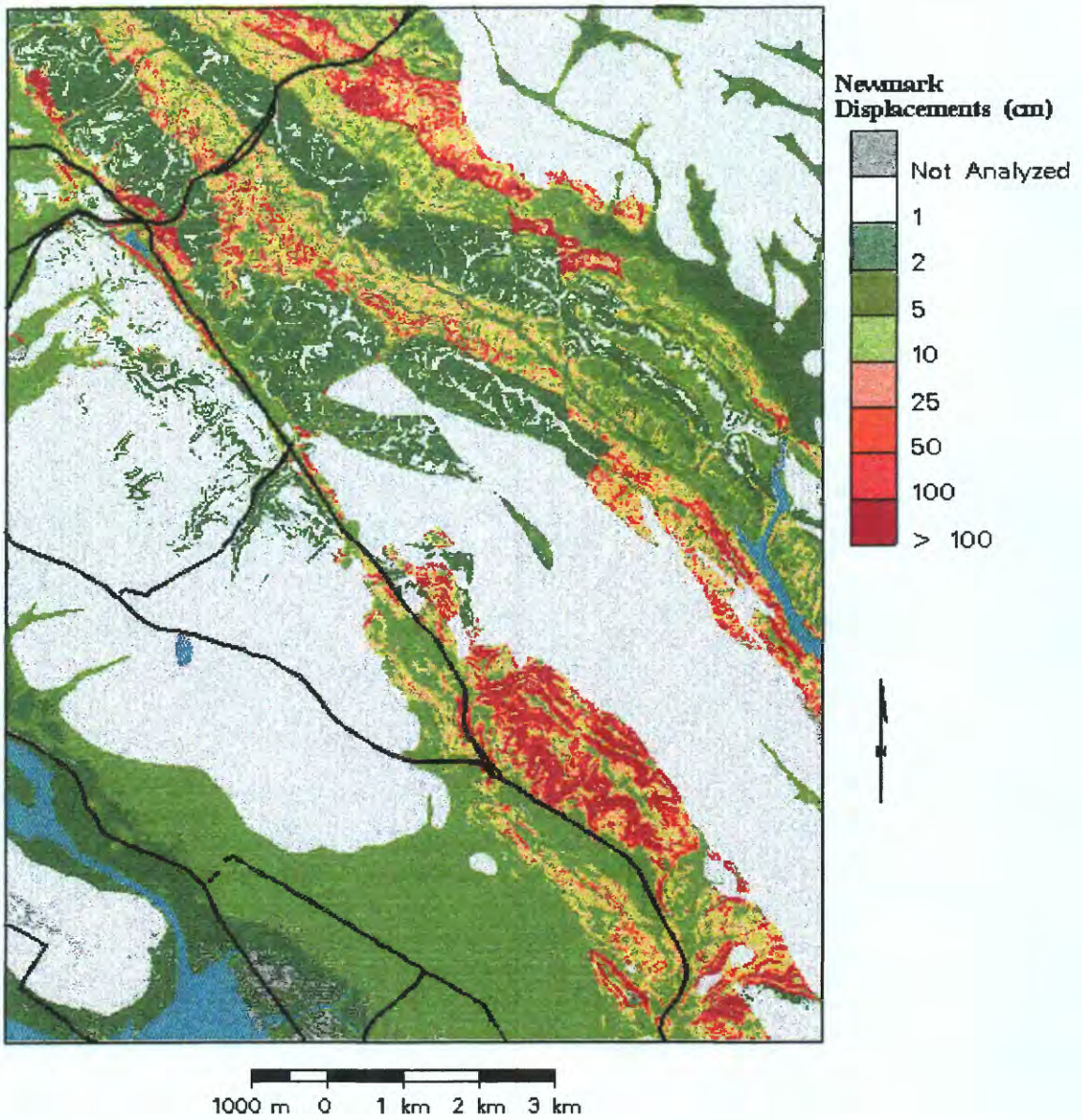

Figure 16. **Jibson and others (1998): saturated conditions.** Map showing predicted Newmark displacements under saturated conditions for the Oakland East quadrangle using the simplified approach of Jibson and others (1998). Newmark displacements predicted for a **M**=7 scenario earthquake on the Hayward fault, California. Major roads shown in black.

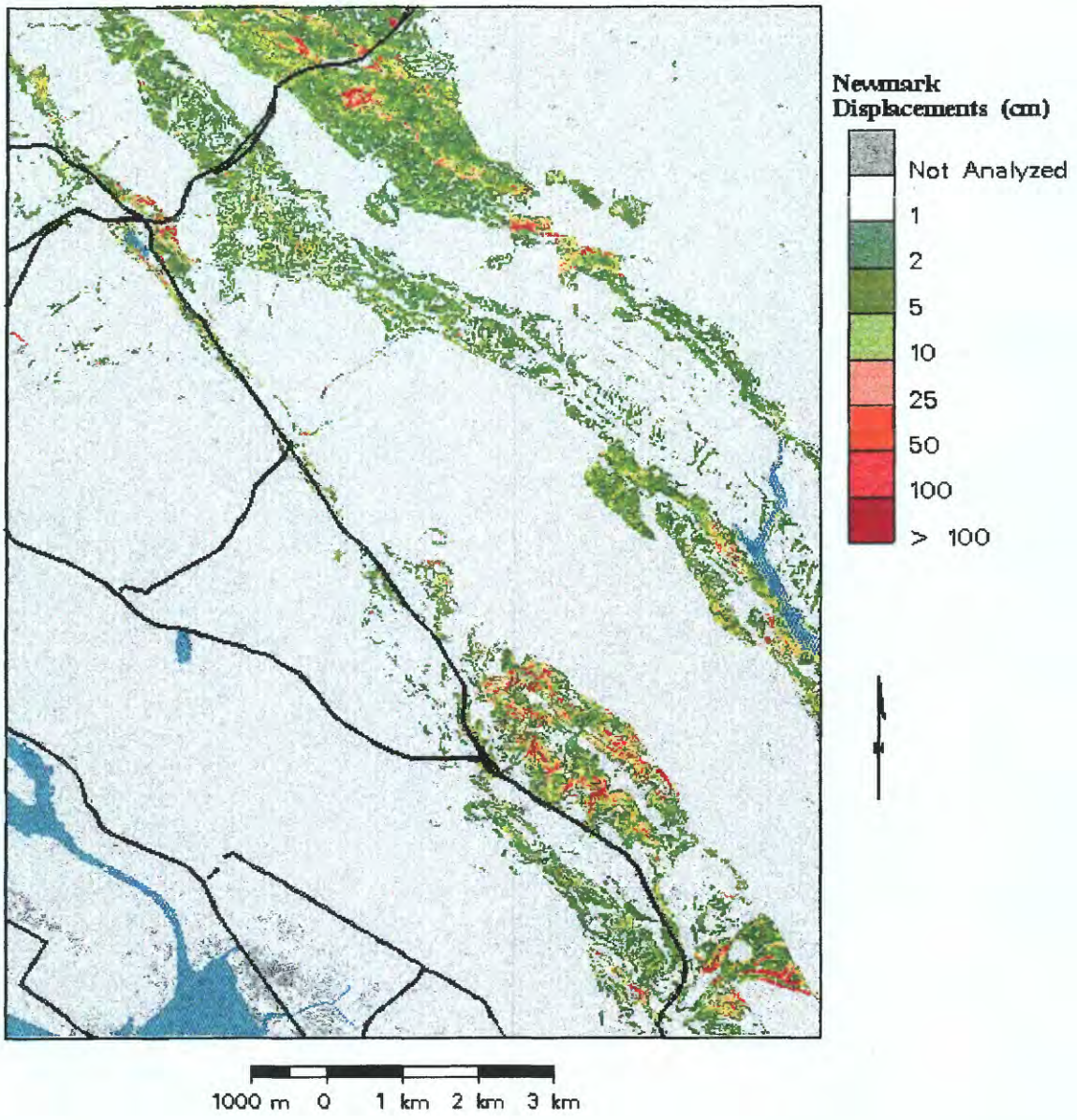

Figure 17. **Miles and Ho (1999): dry conditions.** Map showing predicted Newmark displacements under dry conditions for the Oakland East quadrangle using the double–integration approach with simulated accelerograms. Newmark displacements predicted for a **M**=7 scenario earthquake on the Hayward fault, California. Major roads shown in black.

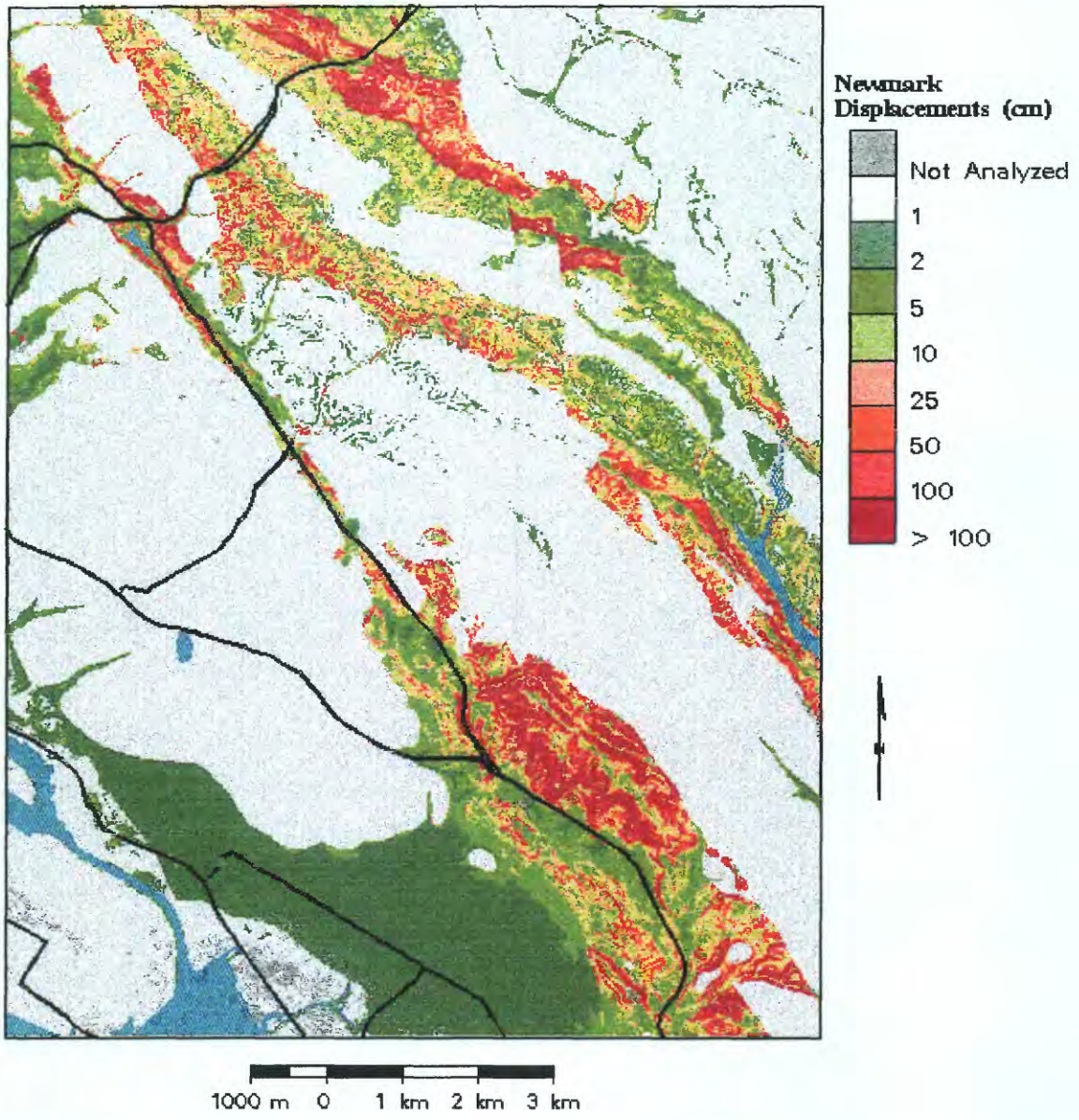

Figure 18. **Miles and Ho (1999): saturated conditions.** Map showing predicted Newmark displacements resulting under saturated conditions for the Oakland East quadrangle using the double–integration approach with simulated accelerograms. Newmark displacements predicted for a M=7 scenario earthquake on the Hayward fault, California. Major roads shown in black.

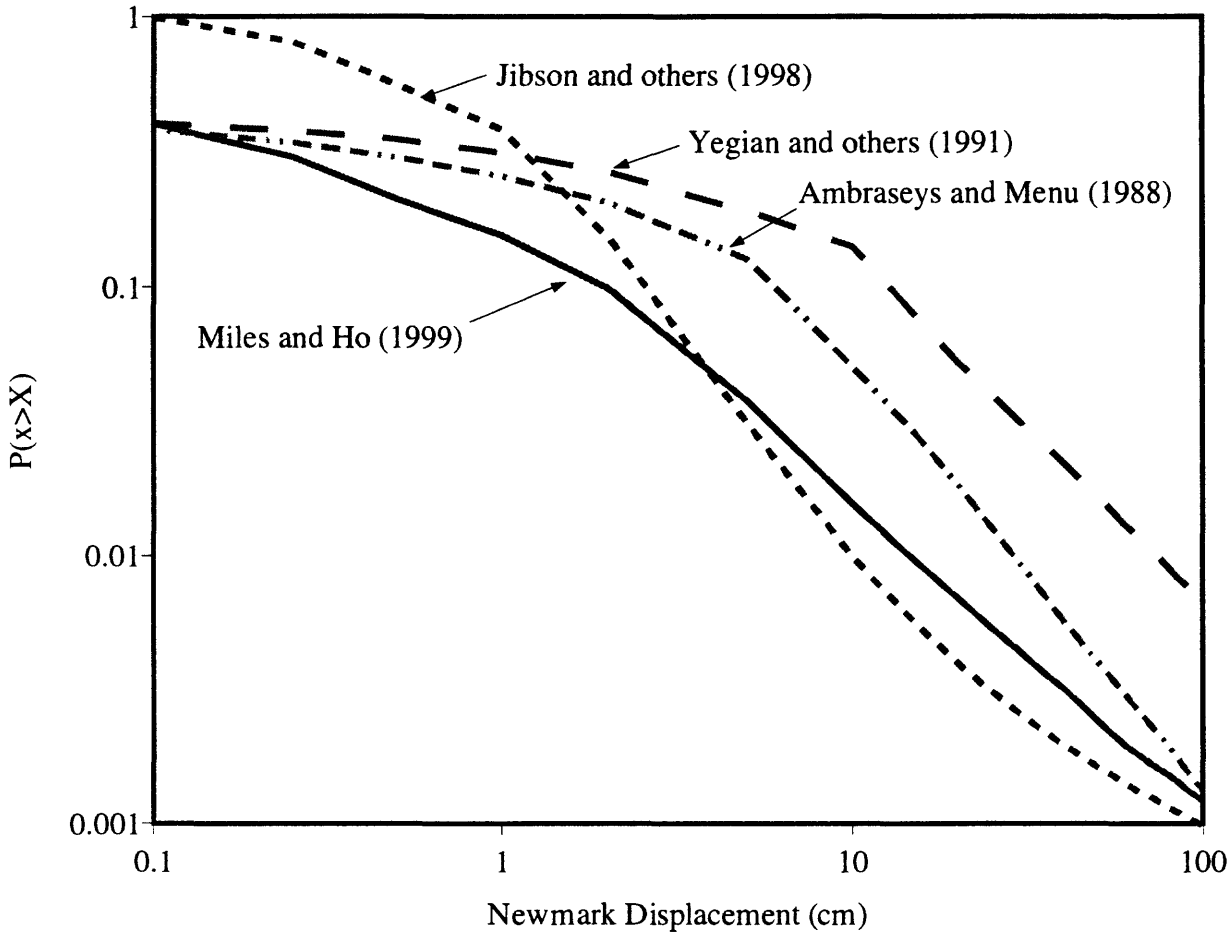

Figure 19. Dry conditions: Cumulative distribution function showing probability of exceedance for Newmark displacements calculated using the four permanent displacement approaches.

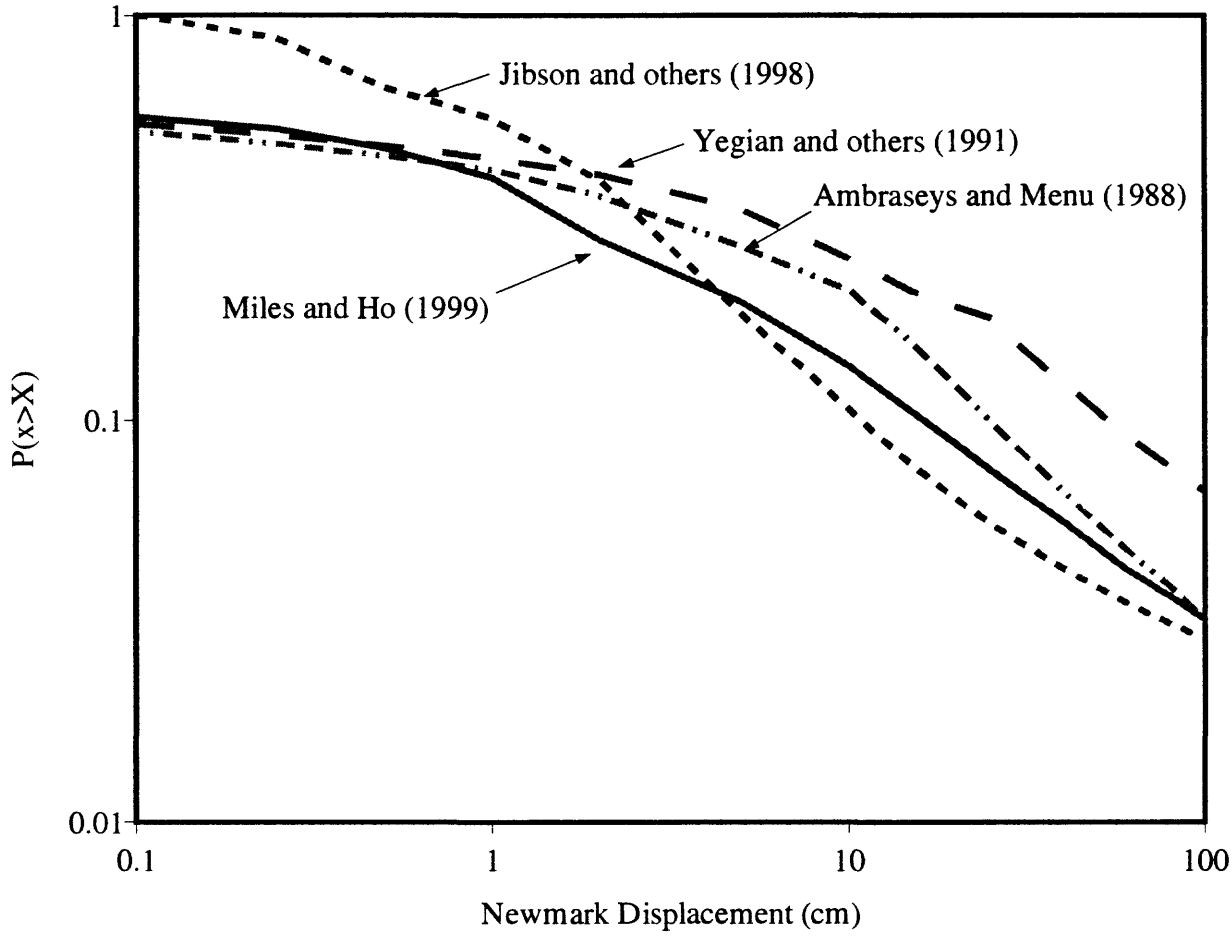

Figure 20. Saturated conditions: Cumulative distribution function showing probability of exceedance for Newmark displacements calculated using the four permanent displacement approaches.